Cellular and molecular control of retinal bipolar cell spatial organization

A Thesis
Presented in Partial Fulfillment of the Requirements for the
Degree of Master of Science
with a
Major in Biology
in the
College of Graduate Studies
University of Idaho
by

Samuel J. Bloomsburg

Major Professor: Peter Fuerst, Ph.D.
Committee Members: Deborah Stenkamp, Ph.D.; Allan Caplan, Ph.D.
Department Administrator: James Nagler, Ph.D.

May 2017

Authorization to submit thesis

This thesis of Sam Bloomsburg, submitted for the degree of Master of Science with a Major in Biology and titled "Cellular and molecular control of retinal bipolar cell spatial organization," has been reviewed in final form. Permission, as indicated by the signatures and dates below, is now granted to submit final copies to the College of Graduate Studies for approval.

Major Professor: _____ Date: _____
Peter Fuerst, Ph.D.

Committee Members: _____ Date: _____
Deborah Stenkamp, Ph.D.

_____ Date: _____
Allan Caplan, Ph.D.

Department
Administrator: _____ Date: _____
James Nagler, Ph.D.

Abstract

The retina is a part of the central nervous system, located within the eye, responsible for detecting and processing the light that passes into the eye. It is contains a huge number of neurons for its size, is highly organized, and is, gram for gram, the most metabolically active tissue in the body. The retina begins development as a clump of neural progenitors pinched off from the anterior end of the neural plate, and ends development with more than 50 cell types, each of which organizes itself with respect to cells of the same type, and with specific afferent and efferent neurons. Proper function of the retina, and hence vision, depends on this organization.

To understand how this organization emerges and is maintained, our lab has taken a genetic and developmental approach to investigating the factors that contribute to patterning and growth. In this work, we investigate the 1) Down syndrome cell adhesion molecule (DSCAM), which has been implicated in developmental cell death, axon guidance, and avoidance and repulsion, and 2) a form of growth-limitation over development which we believe contributes to the accuracy of visual information transmitted by retinal bipolar cells.

In chapter 1, we show that *Dscam* mediates homotypic avoidance during development, and show that it affects neural plasticity in adulthood.

In chapter 2, we present a novel form of growth-limitation. Here we find that bipolar cell axon arbors correlate in size with bipolar cell dendrite arbors. We also find that bipolar cell dendrites do not sample all cones in the retina, and the pattern in which they leave space "un-sampled" is recapitulated by bipolar cell axons, which leave "un-sampled" regions of their own in their own synaptic layer.

In chapter 3, we present a transgenic Cre line, *Pou4f2-Cre*, which we believe to be a useful tool for vision researchers, including ourselves.

Acknowledgements

First, I would like to acknowledge my Major Professor, Peter Fuerst, PhD. You have taught me a great deal of science, and also taught me a lot about the art of teaching and mentorship.

I would like to thank the members of my advisory committee, Deborah Stenkamp, PhD and Allan Caplan, PhD. You are stalwart examples of professionalism as scientists and educators. Pete, Deb and Allan: in a perfect world, my committee would have consisted of exactly you three.

Thank you to all of the members of the Fuerst lab over the last two years: Aaron Simons, PhD, Joshua Sukeena, PhD, Shuai Li, PhD, Yohaniz Ortega-Burgos, Donson Cook-Gallardo, Jamie Doyle, Eric Cliff, Jamie Young, Samuel Billingslea, and CJ Miller. In one way or another, all of you contributed to the work represented here.

Additionally, thank you other staff and faculty who helped me as a graduate student at University of Idaho: Ann Norton, director of the IBEST Optical Imaging Core, James Nagler, PhD, Department Chair, and the staff of the Department of Biological Sciences and the College of Graduate Studies.

Dedication

To Dave.

Table of contents

List of figures

List of tables

Preface

The work in the following document contains multiple-authored work that is shared by Aaron Simmons and Samuel Bloomsburg and is presented in chapters within Simmons' dissertation and Bloomsburg's thesis.

In the chapter "Non-selective OFF bipolar cell plasticity is inhibited by DSCAM mediated enforcement of dendritic and axonal outgrowth in the adult mouse retina," Simmons is the primary author and took lead on conceptualization of the project and oversight of all conducted experiments. Simmons developed the methodologies to visualize and measure bipolar cell morphometrics and discovered DSCAM as a negative regulator of plasticity in non-selective OFF bipolar cells during development through the enforcement of neuron tiling. Bloomsburg assisted with all of the experiments for the project and took lead on experiments associated with bipolar cell axons. Bloomsburg discovered that DSCAM is localized to bipolar cell axons and is required to organize their axon morphologies. Bloomsburg developed methodologies to measure population dynamics of bipolar cell innervation of cones. Together Simmons and Bloomsburg discovered the role of DSCAM in mature neurons is to continually inhibition dendrite and axon outgrowth and removing DSCAM inhibition is sufficient to stimulate synaptogenesis.

In the chapter "Pou4f2 knock-in Cre mouse: A multifaceted genetic tool for vision researchers," Simmons is the primary author and took lead on conceptualization of the project and oversight of all conducted experiments. Simmons mapped out the insertion point of Pou4f2:Cre and explored its mode of action, which depends upon the mouse breeding scheme. Bloomsburg assisted with all of the experiments for the project and took lead on experiments elucidating the developmental expression patterns of Pou4f2:Cre expression pattern within the retina and the brain.

Chapter 1

Non-selective OFF bipolar cell plasticity is inhibited by DSCAM mediated enforcement of dendritic and axonal outgrowth in the adult mouse retina.

Aaron B. Simmons1, Samuel J. Bloomsburg1, Joshua M. Sukeena1, Calvin J. Miller1, Bart G. Borghuis2, and Peter G. Fuerst1,3

1 Department of Biological Sciences, University of Idaho, Moscow, Idaho 83844, USA.

2 Department of Anatomical Sciences and Neurobiology, University of Louisville School of Medicine, Louisville, Kentucky 40202, USA.

3 WWAMI Medical Education Program, University of Washington School of Medicine, Moscow, Idaho 83844, USA.

Abstract

Purpose: Neural populations within the retina organize themselves with respect to neurons of the same type and with respect to afferent and efferent neurons. Understanding how this organization arises is a fundamental goal for developmental biologists who study the eye. Additionally, understanding how this organization is maintained in the face of normal and pathological aging is important to the understanding of diseases of neural retina and to efforts to regenerate retina. In this research, we investigate the role of Down syndrome cell adhesion molecule (DSCAM) in developing and maintaining organization of mouse retinal bipolar cells.

Methods: We use transgenic cre lines to drive population and time specific knockout of *Dscam* in mouse Type 4 OFF cone bipolar cell (BC4). Using fluorescent transgenes and confocal microscopy, we analyzed characteristics of these cells: dendrite and axon arbor areas, degree of overlap with homotypic neighbors, numbers and behavior of dendrite synapses at the cone pedicle, length of dendrites, and localization of DSCAM protein.

Results: We find that DSCAM enforces tiling of BC4 axons and dendrites. Its loss in development is sufficient to cause loss of tiling in BC4s. Its knockout in adulthood is also sufficient to cause BC4s to progressively lose tiling. We also find that BC4s are competent to make additional synaptic connections well into adulthood in mouse, but typically make more connections within an area constrained by homotypic avoidance. Loss of *Dscam* and subsequent loss of tiling is sufficient to allow BC4s to make additional synaptic connections outside of their proper tiled receptive territories.

Conclusions: These findings demonstrate that *Dscam* establishes and maintains organization within the retina, and implicate *Dscam* in neural plasticity: *Dscam* may be a target for retina regeneration therapies.

Introduction

The retina, the neural tissue of the eye, transduces light information (photons) into neurochemical information, processes that information to detect features of vision like color, shape, movement and contrast, and then passes that information to the brain. Within the retina, information passes from the photoreceptors, through the bipolar cells (BCs) and amacrine cells (ACs), to the retinal ganglion cells (RGCs) which are the output neurons of the retina. Each of these cell types have numerous subpopulations, and organize extensively, with themselves and each other (Masland, 2012). Organization is established during development, during which time developing neurons readily extend axons and dendrites and make novel synaptic connections. As development draws to a close, though, retinal neurons lose competency to make novel connections (Thakurela et al., 2015). The ability of mature neurons to make novel contacts in response to cues such as damage and change over the life of the mature organism is called plasticity. Understanding development is crucial to understanding the organization that makes vision possible, and understanding neural plasticity is crucial to understanding injury recovery and degenerative diseases within the nervous system (Fernandez-Hernandez and Rhiner, 2015, Rodriguez and Verkhratsky, 2011, Schmidt and Minnerup, 2016).

In this study we investigate Down syndrome cell adhesion molecule (DSCAM), both for its role in establishing organization over development and as an intrinsic factor that limits plasticity. Our system of study was the mouse Type 4 OFF bipolar cell (BC4), one of 13 bipolar cells in mouse. BC4s establish tiling mosaics by cell type during development (Wässle et al., 2009), and, in the vertebrate retina, are generally considered to have limited plasticity after development is finished at approximately one-month of age (Gibson et al., 2013). These

features made them an ideal neuron population with which to screen factors affecting development and plasticity. Additionally, BC4s are small, and specific transgenes and immunological markers are available for them, which enabled high-quality imaging and specific genetic manipulations (Haverkamp et al., 2008, Lu et al., 2013, Lu et al., 2009). Here, we find 1) that the tiled dendritic and axonal territories of BC4s are enforced by homotypic recognition mediated by DSCAM 2), that WT BC4s retain a surprising degree of plasticity in the mature retina, making novel connections out to at least six-months of age. 3) *Dscam* deletion is sufficient to activate BC4 dendrite outgrowth and increase the number of synapses.

Specifically, BC4 specific knockout of *Dscam* caused loss of tiling in both axons and dendrites, in which *Dscam* localization was characterized. BC4s make more synaptic connections out to six months of age, which in WT are made within the tiled BC4 field. In BC4s that lose *Dscam*, BC4s lose tiling after *Dscam* deletion, and make novel connection in newly gained territory, which was identified through morphological experiments and confirmed by physiology.

I assisted with all experimental work in this research (with the exception of imaging and quantifying single cell data and physiology). I took a lead role in experiments related to axon behavior and outgrowth and quantifying DSCAM localization, and an equal part in characterizing cone synapses, quantifying cell numbers and retinal areas. I took a role in design of experiments and presentation of results, subordinate to authors Simmons and Fuerst.

Materials and Methods

***Mouse Strains and Handling*.** Mice were handled in accordance with protocols approved by the Animal Use and Care Committees at the University of Idaho. In this study, the transgenic mouse line *Dscam*^{tm1Pfu} (referred to as *Dscam*^{FF}) (Fuerst et al., 2012) was used to manipulate *Dscam*. The Cre-reporter mouse Gt(ROSA)26Sortm9(CAG-tdTomato)Hze (referred to as *Ai9*, The Jackson Laboratory, stock no:007909) (Madisen et al., 2010) was used. Two Cre transgenic mouse lines were used: (1) Tg(Htr2a-cre)KM207Gsat (referred to as *5-Htr2a-cre*, MMRRC, stock no:036750) (Lu et al., 2013) and (2) *Pou4f2-cre* (courtesy of Dr. Vann Bennett; Duke University). One GFP transgenic mouse was used: 5-Htr2a-EGFP (referred to as *5-Htr2a-GFP*, MMRRC, stock no:DQ118) (Lu et al., 2009). Mice were maintained on a mixed genetic background containing C57BL/6, C3H, 129, and FVB. Mutant alleles of *Pde6b* were crossed out of colony. Mice were fed ad-libitum and kept on 12h light/dark cycles. A minimum of three retinas from three mice were used in each measurement, unless otherwise stated.

***Genotyping*.** The genotyping of mice followed a procedure as previously described (Li et al., 2015), while the primers used can be found in the following publications: *Dscam*^{FF} (Fuerst et al., 2012); *DscamGOF* (Li et al., 2015); *Ai9* (Madisen et al., 2010); *5-HTR2a-cre* (Lu et al., 2013); *5-HTR2a-GFP* (Lu et al., 2009). All mice taken for study were given a unique alphabetical code that was dissociated from the genotypes to those performing experiments until the data was completely collected and recorded. Tail biopsies were taken from each mouse in the instance that the genotype of a coded retina would need to be verified.

Tissue preparation. Mice were anesthetized using tribromoethanol. Anesthetized mice were perfused with phosphate-buffered saline (PBS), pH 7.4. Eyes were then carefully removed using forceps and dissected in PBS to remove the cornea, iris and lens. Eyes were fixed in 4% paraformaldehyde (PFA) solution for 30 minutes at room temperature and the retina was dissected from the eyecup. Fixed retinas were sunk in 30% sucrose overnight before freezing. Sucrose sunk tissues were placed in Tissue-Tek optimal cutting temperature (OCT) media (Sakura Finetek, Torrance, CA) and frozen by placing the block above liquid nitrogen to rapidly freeze the sample. Retinas were then sectioned at 10 μm and placed onto charged slides. Whole fixed retinas were washed thoroughly in PBS and then stained. All other tissues were fixed in 4% PFA overnight at 4° C and washed thoroughly with PBS. Tissues for cryo-sectioning were handled in the same manner as the retinas.

Microscopy. Micrographs were captured using either a Nikon Spinning Disk confocal microscope or an Olympus Scanning Laser confocal microscope. Images were processed in FIJI (National Institutes of Health, Bethesda, MD, USA) and/or Adobe Photoshop (Adobe Systems, Inc., San Jose, CA, USA). Any changes to brightness or contrast were performed uniformly across the image.

Immunohistochemistry. *Sections:* Tissues were blocked in a blocking solution (5% normal donkey serum, 0.1% Triton X-100 and PBS) for 30 minutes at room temperature. Blocking solution was used to dilute primary antibodies. Sections were incubated in primary antibodies overnight at 4° C. Sections were then washed in PBS at room temperature 3 times prior to secondary staining. Secondary antibodies were also diluted in blocking solution and incubated

overnight at 4° C. Sections were again washed 3 times in PBS at room temperature. DAPI was added to the second wash at a concentration of 1:50,000 from a 1 mg /ml stock. Coverslips were applied using 80% glycerol as a mounting medium. *Whole retinas:* Whole retinas were stained in a similar manner except: blocking solution used was composed of (5% normal donkey serum, 0.4% Triton X-100 and PBS), blocking was performed at 4° C overnight, both primary and secondary incubations lasted 2-4 days at 4° C, and the final wash was performed in 0.4% Triton blocking solution overnight at 4° C.

Antibodies and Stains. *Primary antibodies:* rabbit anti-calbindin (CB-38a, 1:500; Swant, Switzerland); mouse anti-calsenilin (05-756, 1:1000; Millipore, Darmstadt, Germany); mouse anti-DSCAM (MAB36661,1:50; R&D Systems, Minneapolis, MN, USA); mouse anti-dystroglycan (MANDAG2(7D11); 1:500; developed by Morris, G.E., Developmental Studies Hybridoma Iowa City, IA, USA); mouse anti-GFP (75-132, 1:250; NeuroMab, Davis, CA, USA); mouse anti-PKARIIβ (610625, 1:1000; BD Biosciences, San Jose, CA, USA); rabbit anti-TH (AB152; 1:500; Millipore). *Secondary antibodies:* all secondary antibodies were used at 1:500 (Jackson ImmunoResearch, West Grove, PA, USA). *Stains:* 4′,6-diamidino-2-phenylindole (DAPI) (4083, 1:50,000 from 1 mg/mL stock; Cell Signaling Technology); peanut lectin (PNA) (L21409, L32460; 1:500; Molecular Probes, Eugene, OR, USA).

5-Htr2a-cre Targeting Efficiency and Effects. The efficiency of *5-Htr2a-cre* targeting was confirmed by analyzing the percent of RFP+ BC4s in mice carrying *5-Htr2a-cre* and *Ai9* in cryosections of retina counterstained with anti-calsenilin, a marker specific to BC4s. We determined that ~80% of BC4s are targeted by *5-Htr2a-cre,* consistent with what was

previously reported (Figure S1 D-E)(cite). For reporter activity, a minimum of 10 images from at least two retinas gathered from at least two mice analyzed at each time-point.

Cell Counts. *Whole populations:* Eight images (four central, four peripheral), equally sampled from the dorsal, ventral, nasal, and temporal regions, were captured from whole-mount retinas stained with cell type specific markers at 1μm increments along the z-axis. 60x magnification (44,944μm^2 field size) was used to capture BC4s, BC3bs and cones. 20x magnification (160,000μm^2 field size) was used to capture DACs. Image stacks were then imported into FIJI and the cell bodies were manually marked using the multi-point tool. The total number of cells per retina was then calculated by extrapolating the total cells counted in those eight images to the total area of the retina. Retina area was quantified by montage imaging the entire whole-mount retina and using the polygon tool in FIJI. *Thickness of retinal layers:* this was performed as previously described.

Quantifying BC4 axons. For BC4 axons, BC4s were labeled using *5-Htr2a-cre* and *5-Htr2a-GFP*. Axon area and total overlap with neighboring BC4 axons was measured.

Quantifying BC4 dendrite organization at the cone synapse. To quantify the total amount of BC4 dendrites at a cone synapse, BC4s in 3m whole-mount retinas were genetically labeled (*5-Htr2a-cre x Ai9*) and counter stained with anti-calsenilin and PNA. In FIJI, cones contacted by a single genetically labeled BC4 were randomly selected from an image, cropped and then a z-projection was generated that captured all of the PNA and Ai9. Binary masks were created for each channel using the threshold tool and the amount of Ai9 area overlapping with the PNA area was measured. After the measurements were complete, the data was split into cones

with only 1BC4 contact, ≥BC4 contacts and combined data by adding on the calsenilin staining to reveal the entire BC4 population. To quantify the amount of BC4 dendrite crossing at the cone synapse, BC4 dendrites at the cone were traced in FIJI and each BC4/Cone connection was classified as either crossing or not crossing. Dendrites that could not be resolved were considered not crossing even if clumping was evident. The following sample sizes were used: 101(*Dscam*$^{+/+}$) and 108(*Dscam*^{FF}; *5-Htr2a-cre*) BC4/cone contacts for Ai9/PNA overlapping, 63(*Dscam*$^{+/+}$) and 42(*Dscam*^{FF}; *5-Htr2a-cre*) BC4 dendrite crossing at the cone synapse.

"Non-targeted" vs "targeted" cells in *Dscam*^{FF} ; *5-HTR2a-cre* retinas: Because only ~80% of BC4s expressed Cre in *Dscam*^{FF} ; *5-HTR2a-cre* retinas, and because *Ai9* reporter was recombined and began expressing RFP in these retinas, in *Dscam*^{FF} ; *5-HTR2a-cre*; *5-HTR2a-GFP* retinas, it was possible to easily determine which BC4s did or did not have functional DSCAM protein. Yellow cells, cells co-expressing GFP and RFP, were positive for Cre and did not have DSCAM protein. Green cells, cells only expressing GFP, were negative for Cre and did have DSCAM protein. The terms "targeted" and "Non-targeted" refer to Cre-positive BC4s within *Dscam*^{FF} ; *5-HTR2a-cre*; *5-HTR2a-GFP* retinas and Cre-negative BC4s within *Dscam*^{FF} ; *5-HTR2a-cre*; *5-HTR2a-GFP* retinas, respectively.

DSCAM localization. All DSCAM localization was performed in cryo-sections of *Dscam*$^{+/+}$*;5-Htr2a-GFP* retinas by staining them with antibodies against GFP, calsenilin and DSCAM. Confocal images were then taken using a scanning laser confocal microscope at 60x x2 magnification, sampling at 0.5µm increments about the z-axis. Image stacks were then

taken into FIJI where there were analyzed by the following metrics. *DSCAM localization on BC4 dendrites:* dendrite tips and cell bodies of BC4s and DSCAM co-localized to BC4 dendrites were identified and marked using the multipoint tool. This distance from DSCAM puncta to the nearest dendrite tip was measured by tracing from the puncta, along the dendrite, to the terminal. Also, the length of each dendrite was measured in the same way, but from the dendrite tip back to the cell body. *DSCAM co-localization with BC4 axons:* using images stacks, volumes surrounding isolated BC4 axons were identified and all of the DSCAM puncta within that area were marked with the BC4 axon channel hidden. Then the channel was made visible and the puncta co-localized with the axon were recorded. As a control, the BC4 axon channel was flipped about the horizontal axis and the measurement was performed again. A minimum of seven cells were used for each measurement.

Results:

Not all of the results of Simmons et al. 2017 are represented in this results section, though they may be briefly mentioned in the abstract, introduction, and discussion. This section is intended to represent my contribution to the experiments conducted in Simmons et al. 2017. For full results I encourage the reader to peruse Simmons et al. 2017.

DSCAM limits BC4 plasticity by enforcing tiling of dendrite and axon arbors.

A primary feature of BC4s is that axon and dendrite arbors tile – that is, fill space and occupy non-overlapping territories within their respective synaptic layers (Wässle et al., 2009). This allows them to completely and non-redundantly sample all photoreceptors in the retina and pass this information with spatial fidelity to RGCs. *Dscam* deletion in the retina is known to cause defects in defects in tiling and related features of organization, but many prior deletion studies of *Dscam* in the retina led to extreme, widespread disorganization (Fuerst at al., 2008, Fuerst et al.,2009). We manipulated *Dscam* expression we with *5-Htr2a-cre* in $Dscam^{FF}$ retinas, which efficiently targets *Dscam* deletion in BC4s with minimal disruption to retinal organization (Figure 1.1). We characterized and quantified a developmental time-course of $Dscam^{+/+}$ and $Dscam^{FF}$ retinas between p15 and 6m, adding significantly to understanding of *Dscam*'s role in development of a single population of retinal neurons with minimal disruption to other cell types. I encourage the reader to consult Simmons et al. 2017 for more details on these quantifications and results.

Next we turned our attention to BC4 axon arbors. In RGCs, DSCAM function differs in the axons and dendrites: in dendrites it restricts growth and prevents clumping, (Fuerst et al., 2012, Li et al., 2015) but in axons it promotes growth and pathfinding (Bruce et al., 2017).

To test if DSCAM has the same function in BC axons and dendrites we confirmed that DSCAM protein was localized to *Dscam*$^{+/+}$ BC4 axons (Figure 1.2 A-C). Next, we analyzed and compared axon tiling between *Dscam*$^{+/+}$ and *Dscam*^{FF}; *5-Htr2a-cre* retinas (Figure 1.2 D-E). To do this, *Dscam*$^{Non\text{-}Targeted}$ BC4 axons that were isolated and surrounded only by *Dscam*^{Targeted} BC4s were analyzed and compared to *Dscam*$^{+/+}$ BC4 axons. Here it is important to note that DSCAM primarily acts as a homotypic cell adhesion molecule and wild type cells adopt a mutant phenotype next to mutant cells of the same type. In this environment, *Dscam*$^{Non\text{-}Targeted}$ BC4s became statistically larger and overlapped more with neighboring BC4 axons, compared to *Dscam*$^{+/+}$ BC4 axons (Figure 1.2 F-G).

Dscam affects organization at the cone pedicle

During analysis of BC4 dendrites, we noticed that *Dscam*^{Targeted} BC4 innervation of cones was highly disorganized and the dendrites of a single BC4 appeared to clump together, compared to *Dscam*$^{+/+}$ BC4s (Figure 1.3 A). To quantify these changes, the density of dendrites from a single genetically labeled BC4 sampling a single cone was quantified (Figure 1.3 B). These data were then split into whether cones were innervated by 1 or ≥2 BC4s as determined by labeling the entire BC4 population with calsenilin. *Dscam*^{Targeted} BC4 dendrites covered significantly more of the cone, compared to *Dscam*$^{+/+}$ BC4s, while the total number of multiply innervated cones is increased in the *Dscam*^{FF}; *5-Htr2a-cre* retina (Figure 1.3 C). To further measure the organization of BC4 dendrites innervating cones, individual BC4 cone innervations were reconstructed and the proportion of innervations with crossing dendrites were logged (Figure 1.3 D-E). A significant increase in the proportion with crossing dendrites was detected in *Dscam*^{Targeted} BC4s, compared to *Dscam*$^{+/+}$ BC4s. We then mapped out the

location of DSCAM protein along BC4 dendrites and found it to be localized along the distal dendrite and not just at the dendrite terminals (Figure 1.3 F-G). This localization is consistent with a model in which *Dscam* organizes BC4 dendrite tips and synapses on the cone pedicle and also mediates homotypic repulsion and tiling between neighboring BC4s.

BC4 plasticity within the mature retina is inhibited by DSCAM.

Our results showing that *Dscam* was developmentally important for tiling and organization, as well as results (not represented in this chapter; I encourage the reader to consult Simmons et al. 2017) which suggest that BC4s continue modifying and organizing dendrite synapses will into adulthood prompted us to investigate the role of *Dscam* in plasticity of BC4s. To investigate this we targeted late deletion of *Dscam* using *Pou4f2:Cre*, which targets *Dscam* in $Dscam^{FF}$ BC4s a little after one-month of age (see chapter 3 of this work). BC4s in $Dscam^{FF}$; *Pou4f2-cre* retinas were analyzed and compared to littermate controls before and after *Pou4f2-cre* mediated recombination. When measured before recombination, at one-month of age (Figure 1.4 A-D), no significant differences in dendrite area, dendrite overlap, or cones contacted were detected between $Dscam^{FF}$ and $Dscam^{FF}$; *Pou4f2-cre* BC4s (Figure 1.4 I-K), a time point at which a phenotype is clearly observed in the $Dscam^{FF}$; *5-Htr2a-cre* retina. When comparing these BC4s targeted with *Pou4f2-cre* at three and six-months of age (Figure 1.4 E-H), significant increases in all of these measurements were detected (Figure 1.4 I-K). No significant differences in retina area were detected at any of the time-points (Figure 1.4 L). This, together with a similar assay using ER:Cre demonstrates that *Dscam* is required to limit growth throughout the life of the organism. *Dscam* deletion in adulthood allows BC4s to grow outside of their tiled territory

and establish new connections there.

Discussion

In previous studies, our lab has shown that *Dscam* mediates homotypic avoidance and its deletion causes fasciculation of neurites, miss-regulated cell number, and cell spacing defects. (Fuerst et al., 2008, Fuerst et al., 2009, Fuerst et al., 2012, Li et al., 2015) In this research, we took advantage of new tools for targeting genetic manipulations and labelling in a well-defined retinal neuron population, BC4s, which was conducive to screening and quantifying changes in organization in development and plasticity in adulthood. This data this system allowed us to collect gives us insight into *Dscam*, homotypic avoidance, and plasticity. We are excited for additional studies we have planned in this system.

In this study, we showed that *Dscam* enforces dendrite and axon tiling, through homotypic avoidance, independent of organizational and structural changes common in other approaches used to study *Dscam* in the retina.

We showed that BC4s have more innate plasticity than previously thought, and that *Dscam* restrains growth, with its deletion – after development ends – sufficient to restore BC4 growth.

These results shed light on the role of *Dscam* and homotypic avoidance. Additionally, they demonstrate that an important developmental process is not only important during development. This process, homotypic avoidance, maintains the tiling mosaic established during development through the life of the organism.

Along the way, we characterized subcellular localization of DSCAM, supporting its proposed role and function.

Furthermore, though *Dscam* is not expressed in other BC4s, the other BCs share the tiled organization of dendrite and axon arbors found in BC4s. This suggests that similar

mechanisms exist for all of the BC types to prevent overlap between neighboring neurons. A direction for future studies will be to examine what elements are required for homotypic avoidance in these cell types, and if they behave similarly to *Dscam* in development and plasticity. It may be that homotypic avoidance, maintained over the life of the organism, is a common mechanism for regulating neural plasticity.

Additionally, the way in which *Dscam* mediates this homotypic avoidance has yet to be elucidated. An understanding of *Dscam*'s mode of action will be important focus of future studies.

References

Bruce FM, Brown S, Smith JN, Fuerst PG, Erskine L. 2017. DSCAM promotes axon fasciculation and growth in the developing optic pathway. Proc Natl Acad Sci USA. Feb 14;114(7):1702-1707.

Fernandez-Hernandez I, Rhiner C. 2015. New neurons for injured brains? The emergence of new genetic model organisms to study brain regeneration. Neurosci Biobehav Rev. 56, 62-72.

Fuerst, PG, Bruce F, Rounds RP, Erskine L, Burgess RW. 2012. Cell autonomy of DSCAM function in retinal development. Dev Biol, 361, 326-37.

Fuerst PG, Bruce F, Tian M, Wei W, Elstrott J, Fellerm MB, Erskine L, Singer JH, Burgess RW. 2009. DSCAM and DSCAML1 function in self-avoidance in multiple cell types in the developing mouse retina. Neuron, 64, 484-97.

Fuerst PG, Koizumi A, Masland RH, Burgess RW. 2008. Neurite arborization and mosaic spacing in the mouse retina require DSCAM. Nature, 451, 470-4.

Gibson R, Fletcher EL, Vingrys AJ, Zhu Y, Vessey KA, Kalloniatis M. 2013. Functional and neurochemical development in the normal and degenerating mouse retina. J Comp Neurol, 521, 1251-67.

Haverkamp S, Specht D, Majumdar S, Zaidi NF, Brandstatter JH, Wasco W, Wässle H, Tom Dieck S. 2008. Type 4 OFF cone bipolar cells of the mouse retina express calsenilin and contact cones as well as rods. J Comp Neurol, 507, 1087-101.

Li S, Sukeena JM, Simmons AB, Hansen EJ, Nuhn RE, Samuels IS, Fuerst PG. 2015. DSCAM Promotes Refinement in the Mouse Retina through Cell Death and Restriction of Exploring Dendrites. J Neurosci, 35, 5640-54.

Lu Q, Ivanova E, Ganjawala TH, Pan ZH. 2013. Cre-mediated recombination efficiency and transgene expression patterns of three retinal bipolar cell-expressing Cre transgenic mouse lines. Mol Vis, 19, 1310-20.

Lu Q, Ivanova E, Pan ZH. 2009. Characterization of green fluorescent protein-expressing retinal cone bipolar cells in a 5-hydroxytryptamine receptor 2a transgenic mouse line. Neuroscience, 163, 662-8.

Madisen L, Zwingman TA, Sunkin SM, Oh SW, Zariwala HA, Gu H, Ng LL, Palmiter RD, Hawrylycz MJ, Jones AR, Lein ES, Zeng H. 2010. A robust and high-throughput Cre reporting and characterization system for the whole mouse brain. Nat Neurosci. Jan;13(1):133-40.

Masland RH. 2012. The neuronal organization of the retina. Neuron. Oct 18;76(2):266-80.

Rodriguez JJ, Verkhratsky A. 2011. Neurogenesis in Alzheimer's disease. J Anat, 219, 78-89.

Schmidt A, Minnerup J. 2016. Promoting recovery from ischemic stroke. Expert Rev Neurother, 16, 173-86.

Simmons AB, Bloomsburg SJ, Sukeena JM, Miller CJ, Borghuis BG, Fuerst PG. Non-selective OFF bipolar cell plasticity is inhibited by DSCAM mediated enforcement of dendritic and axonal outgrowth in the adult mouse retina.

Thakurela S, Sahu SK, Garding A, Tiwarki VK. 2015. Dynamics and function of distal regulatory elements during neurogenesis and neuroplasticity. Genome Res, 25, 1309-24.

Wässle H, Puller C, Muller F, Haverkamp S. 2009. Cone contacts, mosaics, and territories of bipolar cells in the mouse retina. J Neurosci, 29, 106-17.

Chapter 2

Bipolar cells limit their growth so that their dendrite arbors match their axon arbors in position and size

Samuel J. Bloomsburg1, Aaron B. Simmons1, and Peter G. Fuerst1,2

1 Department of Biological Sciences, University of Idaho, Moscow, Idaho 83844, USA.
2 WWAMI Medical Education Program, University of Washington School of Medicine, Moscow, Idaho 83844, USA.

Abstract

Purpose: In the retina, bipolar cells (BCs) convey information from photoreceptors to retinal ganglion cells (RGCs), the output neurons of the retina. BCs of each type organize themselves into tiled mosaics, in order to sample photoreceptors completely and non-redundantly. Homotypic avoidance plays an important role in establishing this organization during development. The purpose of this research was to investigate another mechanism of organizing bipolar cell axons and dendrites independent of the well-established mechanism of homotypic avoidance.

Method: We measured Type 4 OFF cone bipolar cell (BC4) dendrite and axons arbor characteristics using two fluorescent transgenes and confocal microscopy. We quantified dendrite and axon arbor sizes, and characterized spaces within the outer plexiform layer

(OPL) not sampled by any BC4 dendrites and spaces within the inner plexiform layer (IPL) not sampled by any BC4 axons. These measurements were acquired in the presence and absence of normal homotypic avoidance.

Results: We found correlation of dendrite arbor and axon arbor areas, in both normal homotypic avoidance systems and systems in which is disrupted or is not playing a normal role. We also found that non-sampled regions of OPL tend to overlie non-sampled regions of IPL and correlate with them in size and shape, both in the presence and absence of homotypic avoidance.

Conclusion: These data suggest that BC4s are able to limit their own growth to maintain a correspondence the region sampled by dendrites and the region in which they are making connections with efferent retinal neurons. This suggests that there are additional mechanisms, other than homotypic avoidance, which help bipolar cells establish their dendrite and axon arbors in a way that maintains the accuracy of visual information that they report.

Introduction

The eye is a remarkable piece of biological hardware which mediates vision, humans' dominant sense, and houses the retina. The retina is, gram-for-gram, the hardest working tissue in the body (Ames et al., 1992). This makes sense given the astonishing complexity of what the retina does: transduce light striking the photoreceptors into neurochemical information, and process an amazing number of features of the visual field, which it then passes to the brain.

Anatomically, the vertebrate retina is composed of three cellular layers: the outer nuclear layer, containing photoreceptors; the retinal ganglion layer, containing the output neurons of the retina; and, interposed between these, the inner nuclear layer, which contains the bipolar cells (BCs), the interneurons of the retina. Within the past few decades, vision researchers have realized to an increasing extent the amount of processing of visual information that occurs within the retina. Commensurately, the field has come to understand that bipolar cells, far from passive conduits, play extremely important roles in the visual processing of the retina (for instance, Masland 2009, Euler et al., 2014). This has led to increased interest in bipolar cells among vision scientists. Additionally, BCs have drawn interest as a models system because several features which make them attractive for study: 1) the retina is one of the more easily accessible CNS tissues 2) immunological markers are available for almost all mouse bipolar cells, and there is an increasing array of transgenic labels and tools for doing genetics 3) BCs, of which there are 13 types in mouse, form mosaics and tile by cell type (Wässle et al., 2009).

Like other tiling systems such as *Drosophila* sensory neurons, BCs can be screened and scored for organizational defects. Previously, our lab has investigated just such an

organizational defect: progressive loss of tiling as a result of loss of Down syndrome cell adhesion molecule (DSCAM), which mediates homotypic avoidance (Fuerst et al., 2008, Fuerst et al., 2009, Fuerst et al., 2012, also chapter 1 of this work). Homotypic avoidance offers a convenient explanation for BC tiling: BCs of a type grow until they reach neighbors on all sides, at which point they stop growing. In this research, though, we looked at parameters of individual BCs and of fields of BCs, which suggest that there are other cues which help pattern BC populations.

In our study, we looked at Type 4 OFF cone BCs (BC4) in mouse retina using a combination of transgenes and immunological markers. We invented two indices for this study: correlation of dendrite and axon arbor sizes and "un-sampled" regions in plexiform (synaptic) layers of the retina. Using these indices to look in retina systems where normal homotypic avoidance was not in effect, we make the case for the existence of an active form of growth limitation by BC4s. We think that this active growth limitation should be considered alongside the more established rules of homotypic avoidance and attraction to afferents in efforts to understand the development and organization of BC4s.

In greater detail, we looked at this correlation of dendrite and axon arbor size in two systems in which homotypic avoidance breaks down: 1) regions of sparse BC4 population where tiling is incomplete. Here there exist "un-sampled" regions within plexiform layers and individual BC4s are isolated to some extent. 2) Retinas in which normal homotypic avoidance is lost through genetic ablation of *Dscam*. In all regions of retina, we found that BC4 axon and dendrite arbor sizes vary dramatically, but that axon and dendrite arbor sizes from an individual cell correlate closely. We found that correlation of axon and dendrite arbor size correlation was maintained in isolated BC4s, and in retinas in which BC4 homotypic

avoidance had been lost. Additionally, looking at fields of BC4s, we found that large regions of un-sampled cones in the outer plexiform layer (OPL) correlate in size and shape with overlying regions of inner plexiform layer (IPL) which were devoid of BC4 axons. These un-sampled spaces and the correlation between them were preserved in retinas in which BC4 homotypic avoidance had been lost.

That these features of organization are maintained in isolated BC4s and in BC4s which lack normal homotypic avoidance suggests that there exists an active form of growth limitation which BC4s use to regulate axon and dendrite growth. This growth limitation is not dependent on homotypic avoidance. What the mechanism of this growth limitation is remains to be investigated. Other current research in the field, which demonstrated that BCs that lose excitatory signaling capacity lose dendrite territory to non-signaling-impaired neighbors (Johnson and Kerschensteiner, 2014), suggests to me that the mechanism may depend on signals coming from higher in the visual circuit.

Materials and Methods

Mouse Strains and Handling. Mice were handled in accordance with protocols approved by the Animal Use and Care Committees at the University of Idaho. For genetic manipulation of *Dscam* two transgenic mouse lines were used: *Dscam*^{tm1Pfu} (referred to as *Dscam*^{FF}) (Fuerst et al., 2012) and *DscamGOF* (Li et al., 2015). One Cre-reporter mouse was used: Gt(ROSA)26Sortm9 (CAG-tdTomato)Hze (referred to as *Ai9*, The Jackson Laboratory, stock no:007909) (Madisen et al., 2010). One Cre transgenic mouse was used: Tg(Htr2a-cre)KM207Gsat (referred to as *5-Htr2a-cre*, MMRRC, stock no:036750) (Lu et al., 2013). One GFP transgenic mouse was used: 5-HTR2a-EGFP (referred to as *5-Htr2a-GFP*, MMRRC, stock no:DQ118) (Lu et al., 2009). Rodless (*rd1/rd1*) mice were generated by breeding in and homozygosing *Pde6b* from the C3H inbred line. All other mice were maintained on a mixed genetic background containing C57BL/6, C3H, 129, and FVB. Mutant alleles of *Pde6b* were crossed out of C3H mice. Mice were fed ad-libitum and kept on 12h light/dark cycles.

Genotyping. The genotyping of mice followed a procedure as previously described (Li et al., 2015), while the primers used can be found in the following publications: *Dscam*^{FF} (Fuerst et al., 2012); *DscamGOF* (Li et al., 2015); *Ai9* (Madisen et al., 2010); *5-HTR2a-cre* (Lu et al., 2013); *5-HTR2a-GFP* (Lu et al., 2009). All mice taken for study were given a unique alphabetical code that was dissociated from the genotypes to those performing experiments until the data was completely collected and recorded. Tail biopsies were taken from each mouse in the instance that the genotype of a coded retina would need to be verified.

Tissue preparation. As previously described in chapter 1.

Microscopy. A Nikon DSU spinning disk confocal microscope or an Olympus FluoView scanning laser confocal microscope was used to collect fluorescent micrographs. Images analysis and processing was performed in FIJI (National Institutes of Health, Bethesda, MD, USA). Any changes to brightness or contrast were performed uniformly across the image.

Immunohistochemistry. As previously described in chapter 1.

Antibodies and stains. *Primary antibodies and stains*: Mouse anti-calsenilin (05-756, 1:1000; Millipore, Darmstadt, Germany); mouse anti-GFP (75-132, 1:250; NeuroMab, Davis, CA, USA). *Secondary antibodies:* all secondary antibodies were used at 1:500 (Jackson ImmunoResearch, West Grove, PA, USA). *Stains:* Peanut lectin (PNA) (L21409, L32460; 1:500; Molecular Probes, Eugene, OR, USA). 4,6-diamidino-2-phenylindole (DAPI) (4083, 1:50,000 from 1 mg/mL stock; Cell Signaling Technology).

"Non-targeted" vs "targeted" cells in Dscam^{FF}. *5-HTR2a-cre* retinas: Because only ~80% of BC4s expressed Cre in *Dscam^{FF}* ; *5-HTR2a-cre* retinas, and because *Ai9* reporter was recombined and began expressing RFP in these retinas, in *Dscam^{FF}* ; *5-HTR2a-cre*; *5-HTR2a-GFP* retinas, it was possible to easily determine which BC4s did or did not have functional DSCAM protein. Yellow cells, cells co-expressing GFP and RFP, were positive for Cre and did not have DSCAM protein. Green cells, cells only expressing GFP, were negative for Cre and did have DSCAM protein. The terms "targeted" and "Non-targeted" refer to Cre-positive BC4s within *Dscam^{FF}* ; *5-HTR2a-cre*; *5-HTR2a-GFP* retinas and Cre-negative BC4s within

Dscam^{FF} ; *5-HTR2a-cre*; *5-HTR2a-GFP* retinas, respectively.

Analysis of BC4 axons and dendrites. Fields of BC4s were imaged from axon to dendrite. On both Nikon and Olympus microscopes, images were taken with 60x objective. On Nikon system, fields were roughly 125x175 microns. On Olympus system, images were either 212x212 microns or 106x106 microns. Images were taken of central retina, peripheral retina, and middle retina (roughly halfway between central and peripheral). Dendrite and axon tips were identified using either GFP or a combination of GFP and RFP. To calculated dendrite and axon arbor areas, convex polygons were drawn around all dendrite or axon tips from a given BC4, BC4 identity was confirmed with calsenilin. This analysis was performed for as many BC4s within the field as possible. In the case of WT retinas, this often resulted in reconstruction of the entire field. Axons from each image were analyzed independently from dendrite in order to minimize the possibility of axon area biasing dendrite area or vice versa.

Analysis of un-sampled regions. All axons and dendrite arbors in an image were drawn as above. When it was not possible to resolve two or more neighboring cells, a convex polygon was drawn around all non-resolvable cells. Large (>200um^2), continuous areas that did not have BC4 dendrites within them, that is "un-sampled regions of OPL," were traced and measured in FIJI. Large (>200um^2), continuous areas that did not have BC4 axons within them, that is "un-sampled regions of IPL," were traced and measured in FIJI.

Isolation score. 1) "Room to grow" percentage: regions of the convex polygon surrounding the dendrite arbor of a BC4 were evaluated on whether there was another BC4 immediately adjacent (that is, capable of restricting growth by homotypic avoidance). Portions of the

perimeter convex polygon where there was not such a cell were classified "room to grow" portions of perimeter. "Room to grow percentage" was calculated as 100% * ("room to grow" perimeter length) / (total convex polygon perimeter length). 2) Binning: analyzed dendrites were binned based on percentage of "room to grow" perimeter out of the total perimeter of the convex polygon. "Room to grow %" < 25% was scored 0; 25% < "room to grow %" < 37.5% was scored 1; 37.5% < "room to grow%" <62.5% was scored 2, 62.5% < "room to grow %" <87.5% was scored 3, 87.5% < "room to grow %" was scored 4. 3) Axon score: this same protocol (steps 1 and 2) was performed for axons to give an axon isolation score. 4) Composite score: a composite score was simply the dendrite score added to the axon score. To be considered isolated/partially isolated, a cell needed an axon score of at ≥1 and a dendrite score of at least ≥1. Thus, isolation scores for BC4s in "isolated/partially isolated" assays ranged from 2 to 8.

"Functional" isolation score: For *DscamFF* retinas, non-targeted cells from *Dscam*^{FF} ; *5-HTR2a-cre*; *5-HTR2a-GFP* retinas were selected for analysis. The assay was applied as above, but only paying attention to non-targeted cells and ignoring targeted cells. That is, perimeter on which a green cell bordered a red cell (or more likely was overlapped by a red cell) was considered "room to grow" perimeter. Only perimeter on which a green cell bordered another green cell was considered not-"room to grow" perimeter.

Results

Identifying BC4s in fluorescent retina systems

5-Htr-GFP and *5-Htr-cre* linked to the ai9 reporter were used to label BC4s. In both *Dscam*^{FF} and WT retinas, *5-Htr-cre* was expressed in ~80% ± 10% of BC4s, as determined by ai9 reporter activity (Lu et al., 2013, also chapter 1 and Simmons et al., 2017). In WT retinas, this led to expression of RFP from the *Ai9* reporter, whereas in *Dscam*^{FF} retinas this led to expression of RFP and recombination and knockout of *Dscam* (Fuerst et al., 2012). In both *Dscam*^{FF} and WT retinas, *5-Htr-GFP* was expressed in >95% of BC4 (Lu et al., 2009). We confirmed the identity of BC4s using the calsenilin antibody, which is specific for BC4s in the outer half the inner nuclear layer (Wässle et al., 2009). (Figure 2.1, A-A’’’) This combination of RFP, GFP, and calsenilin was used to map dendrite territories, and a combination of GFP and RFP was used to map axon territories, as calsenilin is not specific for BC4 processes within the IPL.

Correlation between size of BC4 dendrite and axon arbors

Bipolar cells convey information from photoreceptors to retinal ganglion cells (RGCs). Preservation of visual acuity would require that the input dendritic fields of bipolar cells (BCs) correlate with their output axonal fields. To test if BCs coordinate regulation of axon and dendrite field sizes we measured fields of BC4s from dendrite to axon. Using FIJI, dendrite and axon tips were identified in 3 dimensional space and their locations recorded. Once all tips had been identified, a convex polygon was drawn which overlay all dendrite or axon tips, yielding a 2 dimensional representation of the territory of the dendrite or axon arbor in the OPL or IPL, respectively (Figure 2.2 B’-B’’’’, 2.2 A’-A’’’’, respectively). Careful work

on well-stained wild type retinas could result in reconstruction of all axon and dendrite territories within an image (Figure 2.2 B and 2.2 C). As will be seen later, this was not always possible to accomplish in *Dscam*^{FF} retinas, due to loss-of-tiling which generated irresolvable tangles of neurites. In WT retinas, we found that the size of dendrite arbors correlated with size of axon arbors. Even within a single 100x100um field, cells with large dendrites also tended to have larger axons (Figure 2.4 A-C)

Density Gradient and "un-sampled" areas of the outer plexiform layer

In collecting this BC4 axon-to-dendrite data for this study, we imaged BC4s across different regions of the retina. When we did this we observed that BC4 density drops dramatically in going from central to peripheral retina (Figure 2.3 A and B). In regions of low density, we found cones, even regions of cones, which were not sampled by BC4s, (Figure 2.3 B). This finding of un-sampled regions of outer plexiform layer (OPL) surprised us given consensus within the field that BCs tile (Wässle et al., 2009, among others). As we continued, we were surprised by how common it seemed to be. We sought to ensure that this finding was not due to BC4s which failed to express GFP, so we confirmed BC4 identity with calsenilin staining and confined analysis to fields in which 100% of BC4s expressed GFP, and verified that un-sampled OPL was present and fairly common.

In these sparse regions, we observed that BC4s seem to reach a maximal size. BC4s which did not touch a neighboring BC4 and thus had room to grow, based on a homotypic avoidance model, did not grow to sample adjacent cones. On measuring BC4s, none were found to exceed a dendrite arbor area of 1500 um^2, and it was rare to find one that exceeded 1000um^2. Even when BC4s lost homotypic avoidance altogether (*Dscam*^{FF}; *5-Htr-cre*

retinas) they rarely exceeded this size (Figure 2.3D).

Gain of Function: In addition to this, we explored arbor sizes and empty space in *Dscam*^{GOF} (Figure 2.3 C). *Dscam*^{GOF} is known to cause dramatic reduction in numbers of retinal neurons (Li et al., 2015), including in BC populations. Early on, we hypothesized that, due to the depletion, BC4s would be much larger in *Dscam*^{GOF} retinas. Instead we found that the sparse BC4s did not exceed normal range of sizes for BC4s in WT retina (Figure 2.3 D), typically did not grow until they touched homotypic neighbors, and left large numbers of cones un-sampled (Figure 2.3C).

Characterization of "un-sampled space"

Having found regions where tiling within the OPL was incomplete, we turned our attention to the IPL, where we found regions that did not seem to have any BC4 axons within them – un-sampled regions of IPL. We reconstructed all dendrite arbors in these fields, and then quantified un-sampled regions of OPL by drawing polygons around continuous regions that were not included in any dendrite arbor. Then we reconstructed all axon arbors and quantified un-sampled regions of IPL. We found that there was correlation between un-sampled OPL area and un-sampled IPL area. Large regions of un-sampled cones tended to overlie large regions of un-sampled IPL area and small regions of un-sampled cones tended to overlie small regions of un-sampled IPL area. Additionally, we observed that these un-sampled OPL-IPL pairs tended to resemble each other in shape (Figure 2.4 D-E).

"Isolated/Partially isolated" BC4s

This un-sampled space was surprising to us given the tiling/ homotypic avoidance

model. But its preservation between OPL and IPL made sense from a preserving visual acuity perspective. It would seem to be a bit maladaptive to not sample a region of cones, but it would possibly be more detrimental for vision as a whole if a BC4 axon was providing input to RGCs about a region of photoreceptors that the BC4 was not actually contacting. But the mechanism by which BC4s were leaving a region un-sampled, in both OPL and IPL, struck us as an open question. To try to answer it, we next focused attention on BC4s that bordered un-sampled regions. We had observed the phenomena of dendrite arbor and axon arbor size correlation without reference to empty space, and we were curious to see how cells bordering un-sampled space would behave. Did BC4s bordering un-sampled regions simply grow to the maximum size, attempting to fill empty space but unable to do so? If so, empty space could be attributed to some circumstance in development that left BC4s at an insufficient density to cover space. In this way empty space could be preserved, and not sampling the space would be a passive process from a BC4 perspective. However, in BC4s bordering un-sampled space, we found that there was a large range of arbor sizes, and that these cells also had a correlation between dendrite and axon arbor sizes. Cells were not growing to the extreme of BC4 growth capacity; their sizes varied, and dendrite and axon arbor sizes varied together (Figure 2.5 A-C). To further investigate this finding, we scored cells according to how isolated they were – how much of their arbor perimeter bordered un-sampled space (Figure 2.5 A' and B') – and found that degree of isolation did not seem to affect degree of dendrite arbor size correlation with axon arbor size. BC4s with different isolation scores seemed to lie on the same trend line, and a broad range of sizes existed for cells at all levels of isolation (Figure 2.5 D and E). This suggested to us that avoidance of un-sampled space was an active process from the perspective of a BC4 bordering un-sampled space.

Correlation of between size of BC4 dendrite and axon arbors in *Dscam*^{FF} retina

In another, concurrent line of experiments to try to understand if the correlation between dendrite and axon arbor sizes was a result of homotypic avoidance or rather represented a different process, we looked at retinas in which homotypic avoidance was lost in BC4s through BC4 selective deletion of *Dscam*, to explore how loss of homotypic avoidance would affect correlation. Originally, based on a tiling model built on homotypic avoidance, we expected loss of *Dscam* to result in more-or-less random growth, which would be predicted to un-link axon and dendrite growth. Instead we found that there was a correlation between dendrite and axon arbor sizes in *Dscam*^{FF} retina. Compared to WT retina, R^2 was less. However, the fact that there was still a fairly strong correlation between dendrite arbor and axon arbor size indicated that correlation was not dependent, or at least not entirely dependent, on homotypic avoidance (Figure 2.6 A, B, and E).

Size range and maximal size in *Dscam*^{FF} retina

When we began looking at BC4s in *Dscam*^{FF} retinas we wondered, as we did when we began looking at WT BC4s bordering empty space, if BC4s would just all grow to a maximal size in the absence of neighbors that could inhibit their growth. We found that this was not the case. We found that arbor size range stayed approximately the same (a range of 1039.3um^2 for WT, 1007.8um^2 for *Dscam*^{FF}) (also see Figure 2.3 D), though the average shifted up somewhat (mean 547.7, median 529.9 for WT; mean 637.6, median 578.2 for *Dscam*^{FF}). However, we soon developed another way of looking at the phenomenon of isolation in the *Dscam*^{FF} retina which more precisely mirrored our isolated BC4 assay.

"Functionally isolated" cells in Dscam^{FF} maintain dendrite/axon correlation

One feature of our transgenic system was that *5-Htr-cre* was only expressed in ~80%±10% (Lu 2013, chapter 1 and Simmons 2017 manuscript) of BC4s. This meant that in the *Dscam^{FF}* retina not every BC4 lost *Dscam*; there were "targeted" and "non-targeted" cells. Furthermore, because the same cre that mediated knockout of *Dscam* also activated the RFP expression from the *Ai9* reporter, it was easy to identify targeted and non-targeted cells. Because of this, we could look at the behavior of a WT cell in a population that had lost homotypic avoidance.

However, because ordinarily DSCAM functions in homotypic avoidance by homophilic binding of DSCAM extracellular domains, a non-targeted BC4 does not repel a targeted BC4 any more than a targeted BC4 repels any other BC4. Non targeted cells will repel processes of other non-targeted cells, but not repel or be repelled by targeted cells.

Consequently, from the homotypic avoidance perspective, a non-targeted BC4 surrounded by targeted BC4s is "functionally isolated" – it should behave as a BC4 with "room to grow" on all sides. With this in mind, we performed our "isolated cell assay" on non-targeted BC4s in *Dscam^{FF}*; *5-Htr2a-Cre* retinas. We found that these functionally isolated cells exhibited a range in arbor sizes from 322.1 um^2 to 1075.4, and high correlation between dendrite arbor and axon arbor size (Figure 2.7).

Characterization of "un-sampled space" in *Dscam^{FF}* retina

Next, we investigated un-sampled space in *Dscam^{FF}* retinas, to see if loss of homotypic avoidance would affect quantity or behavior of OPL or IPL un-sampled space. Given our prior expectation of, overall, less restrained and more random growth in *Dscam^{FF}*

retina, we also expected empty spaces to be smaller, with less correlation between size and shape of dendrite arbor and axon arbors. In fact, we continued to find un-sampled space in the *Dscam*^{FF} retina; empty space was if anything increased, and a high degree of correlation between OPL and IPL un-sampled space was observed. While growth is certainly less regulated in BC4s that lose *Dscam* and with it normal homotypic avoidance, mechanisms continued to be in place to preserve empty space (Figure 2.6 C, D, and F).

Discussion

The forest and the trees: a word on the model system and measurements used

In this research, the combination of fluorescent transgenes and reporter lines and cell-type-specific immunological markers allowed us to look at individual cells with good resolution, and to look at populations at the same time. Additionally, our approach of looking at entire cells (dendrite to axon) offered additional information that is not available from imaging only dendrites or axons.

Approaches that look at single cells, or single parts of single cells, risk losing sight of the forest for the trees. Approaches that look at populations but lack resolution to see single cells can't see the trees. The two features that we measured – paired axon and dendrite arbor sizes, un-sampled OPL and un-sampled IPL regions – reveal things which aren't apparent in either a population only approach, or a single cell only approach, or a dendrite only approach, or an axon-only approach. Our results depended on this approach, and the technology that enabled it.

BC4 growth self-limitation: a revised paradigm

In this research we have proposed that BC4s have some developmental mechanism for limiting their own growth, despite the presence of attractive afferents and independent of the well-established mechanism of homotypic avoidance. One of our main findings in this paper was a surprisingly common and organized un-sampled space. As far as we know, leaving regions of cones un-sampled does not serve any adaptive function in the vertebrate retina. Rather, we think this phenomenon is a particular case of a general rule about bipolar cells growth, and we think that our other main finding, correlation between dendrite and axon arbor

size, sheds some light on what this rule might be. BC4 dendrite arbors adjacent to regions of un-sampled cones vary in size, but the size of their dendrite arbors correlates closely with axon arbor size. This suggests to us that axons may be exerting influence over dendrite growth. This in turn suggests higher-circuit involvement, possibly of the type described in Kerschensteiner 2014. That the correlation between dendrite and arbor size appears similar throughout the retina suggests that this rule is in effect throughout the retina. One can easily crease models which provide a mechanism for such a rule. Suppose, for instance, that BC4 axons receive some neurotrophic factor from axons, and stop growing when they receive sufficient neurotrophic factor, with stochasticity in how much neurotrophic factor is enough or variable neurotrophic factor distribution to explain different sizes.

Hypothetical models aside, our results do suggest that BC4s restrain themselves from growing in a particular direction when there isn't a neighbor there to repel them, which flies in the face of what we think about how BCs organize. BC organization studies have tended to focus on how the BCs target afferents, and how BCs influence homotypic neighbors. We think that our findings suggest a model in which BCs grow based on 1) a permissive cue, possibly derived from higher in the visual circuit, 2) attractive cues from photoreceptors, and 3)homotypic avoidance cues (or lack thereof) from their neighbors.

Wild speculation and further directions

Admittedly, while the research represented here provides evidence that there is a self-limitation-of-growth rule, it does not provide much evidence for any model or mechanism underlying or providing a rationale for said rule. However, the next planned experiments will help understand the mechanism, whether in support of the neurotrophic factor model briefly

proposed in this discussion or something much different. The next two near-term, planned experiments are 1) careful depletion of RGCs and photoreceptors and 2) careful depletion of BC4s. If in fact BC4 axon arbor territories are established by a neurotrophic factor received from synapses with RGCs, we would expect a developmentally early (before BC maturation) depletion of RGCs to lead to a reduced population of BC4s, probably with larger arbors. A later depletion of RGCs (after some degree of BC4 maturation) would be less predictable, even if large parts of the neurotrophic factor model are true. We predict BC4s to die if their efferent RGC is killed. But alternatively, this could cause BC4 axons to exploring for RGC dendrites. Or perhaps BC4s whose efferent RGCs are killed would maintain axon arbors in the same place, but lose dendrite arbor territory to innervated neighbors. Many imaginable results of from this experiment involve imbalance of growth between axons and dendrites, resulting in a loss of correlation between them. In short, we would expect BC4s in a RGC depleted retina to be abnormal, in contrast to rodless retinas, in which BC4 territories look pretty normal.

In contrast, a BC4 depletion would be expected – if nothing else – to preserve the correlation between dendrite and axon arbor size. If this were not the case, it would call into question not only our neurotrophic factor model but the growth limitation rule presented in this paper. BC4 depletion retinas would also be expected to have more empty space, and it would be extremely interesting to see the response to newly-created empty space in a mature BC4 field. An experimental readout of great interest here would be whether BC4s grow into un-sampled space created by the deaths of other BC4s. If they grow at all, it would be interesting to note at what growth proceeds, and whether axons lead the way followed by dendrites, or vice versa. Looking at a time course of BC4 depletion retinas, perhaps 1 week, 2

weeks, and 1 month after BC4 depletion, would answer these questions.

One more interesting and potentially informative series of experiments further down the pipeline would be to alter microtubule dynamics, which would potentially affect axon growth as well as retrograde (axon-to-cell-body) signaling. Results from all these experiments will help confirm the growth limitation rule proposed in this paper and build a model to explain it.

The reason that we want to build a model is as follows. Reiterating slightly, one of our main findings in this paper was correlation in size of dendrite and axon arbors. A potential ramification of this is that a great deal of spatial acuity is built into the physical layout of BC4 axons and dendrites. The mechanism underlying the correlation could help understand its purpose. For instance, if it turns out that RGCs help establish this spatial acuity, it would imply that it is important for processing of information by RGCs. If higher visual circuitry is involved in patterning BC4s, this research would join a growing body of work suggesting that BCs are engaged in cross talk with the visual circuit, improving our understanding of the development and role in visual processing of the retinal bipolar cell.

References

Ames A 3rd, Li YY, Heher EC, Kimble CR. Energy metabolism of rabbit retina as related to function: high cost of Na+ transport. J Neurosci. 1992 Mar;12(3):840-53.

Euler T, Haverkamp S, Schubert T, Baden T. Retinal bipolar cells: elementary building blocks of vision. Nat Rev Neurosci. 2014 Aug;15(8):507-19.

Fuerst PG, Bruce F, Rounds RP, Erskine L, Burgess RW. Cell autonomy of DSCAM function in retinal development. Dev Biol. 2012 Jan 15;361(2):326-37.

Fuerst PG, Bruce F, Tian M, Wei W, Elstrott J, Feller MB, Erskine L, Singer JH, Burgess RW. DSCAM and DSCAML1 function in self-avoidance in multiple cell types in the developing mouse retina. Neuron. 2009 Nov 25;64(4):484-97.

Fuerst PG, Koizumi A, Masland RH, Burgess RW. Neurite arborization and mosaic spacing in the mouse retina require DSCAM. Nature. 2008 Jan 24;451(7177):470-4.

Johnson RE, Kerschensteiner D. Retrograde plasticity and differential competition of bipolar cell dendrites and axons in the developing retina. Curr Biol. 2014 Oct 6;24(19):2301-6.

Li S, Sukeena JM, Simmons AB, Hansen EJ, Nuhn RE, Samuels IS, Fuerst PG. DSCAM promotes refinement in the mouse retina through cell death and restriction of exploring

dendrites. J Neurosci. 2015 Apr 8;35(14):5640-54.

Lu Q, Ivanova E, Ganjawala TH, Pan ZH. Cre-mediated recombination efficiency and transgene expression patterns of three retinal bipolar cell-expressing Cre transgenic mouse lines. Mol Vis. 2013Jun 12;19:1310-20.

Lu Q, Ivanova E, Pan ZH. Characterization of green fluorescent protein-expressing retinal cone bipolar cells in a 5-hydroxytryptamine receptor 2a transgenic mouse line. Neuroscience. 2009 Oct 6;163(2):662- 8.

Madisen L, Zwingman TA, Sunkin SM, Oh SW, Zariwala HA, Gu H, Ng LL, Palmiter RD, Hawrylycz MJ, Jones AR, Lein ES, Zeng H. A robust and high-throughput Cre reporting and characterization system for the whole mouse brain. Nat Neurosci. 2010 Jan;13(1):133-40.

Masland RH. The neuronal organization of the retina. Neuron. 2012 Oct 18;76(2):266-80.

Simmons AB, Bloomsburg SJ, Sukeena JM, Miller CJ, Borghuis BG, Fuerst PG. Non-selective OFF bipolar cell plasticity is inhibited by DSCAM mediated enforcement of dendritic and axonal outgrowth in the adult mouse retina.

Wässle H, Puller C, Müller F, Haverkamp S. Cone contacts, mosaics, and territories of bipolar cells in the mouse retina. J Neurosci. 2009 Jan7;29(1):106-17

Chapter 3

Pou4f2 knock-in Cre mouse: A multifaceted genetic tool for vision researchers.

Aaron B. Simmons1, Samuel J. Bloomsburg1, Samuel A. Billingslea1, Morgan M. Merrill1, Shuai Li1, Marshall W. Thomas2 and Peter G. Fuerst1,3

1 Department of Biological Sciences, University of Idaho, Moscow, Idaho 83844, USA.

2 Department of Biology, Brigham Young University—Idaho, Rexburg, Idaho 83460, USA.

3 WWAMI Medical Education Program, University of Washington School of Medicine, Moscow, Idaho 83844, USA.

Published June 23 2016 in Molecular Vision vol. 22 p705-717

Abstract

Purpose: A transgenic mouse that expresses Cre recombinase under control of the *Pou4f2*-promoter (also referred to as *Brn-3b and Brn-3.2*) was characterized. *Pou4f2* expression has been reported in a subset of retinal ganglion cells (RGCs) in the retina, in the midbrain and in the germ line. In this study we characterize the expression pattern of this Cre-recombinase line and report its utility in targeted deletion, temporal deletion, RGC depletion and germ line targeting, which can be regulated by the sex of the Cre-carrying mouse.

Methods: *Pou4f2*^{Cre} was mapped by utilizing a combination of polymerase chain reaction

(PCR) and sequencing of PCR products to better understand the construct and to locate where it was inserted within the *Pou4f2* locus. Cre expression patterns were examined by crossing *Pou4f2*$^{Cre/+}$ mice to Cre reporter mice. Immunohistochemistry was used to further define the pattern of Cre expression and Cre-mediated recombination within the retina, brain and other tissues.

Results: An IRES-Cre cassette was inserted into the *Pou4f2* gene disrupting normal gene function, as verified by depletion of RGCs in mice homozygous for the insert. *Pou4f2*^{Cre} expression was observed in the retina, brain, peripheral neurons and the male germ cells. Germline recombination was observed when the sire carried both the Cre and the target for recombination. In all other breeding schemes, recombination was observed within subsets of cells within the retina, brain, intestines, heart and gonads. In the retina, Cre efficiently targets recombination in neurons within the retinal ganglion cell layer, inner nuclear layer and a small percentage of photoreceptors, activity that has not been previously reported. Unlike most other Cre lines active in the inner retina, recombination in Müller and other glia was not observed in mice carrying *Pou4f2*^{Cre}. Within visual centers of the brain, Cre targets recombination in about 15% of cells within the superchiasmatic nucleus, lateral geniculate nucleus and superior colliculus.

Conclusions: *Pou4f2*^{Cre} provides multiple uses for the vision researcher's genetic toolkit. First, *Pou4f2*^{Cre} is a knock-in allele that can be used to eliminate *Pou4f2*, resulting in depletion of RGCs. Second, expression of Cre in the male germ cells makes this strain an efficient germline activator of recombination, for example to target loxP-flanked sequences in the

whole mouse. Third, *Pou4f2*^{Cre} efficiently targets RGCs, amacrine cells, bipolar cells, horizontal cells and a small number of photoreceptors within the retina, as well as visual centers in the brain. Unlike other Cre recombinase lines that target retinal neurons, no recombination is observed in Müller or other retinal glia. These properties make this Cre recombinase line a useful tool for vision researchers.

Introduction

Targeted manipulation of the genome has greatly improved our ability to study the roles of genes in development. Cre-lox technology, in which Cre recombinase excises DNA sequence flanked by loxP sites, allows for targeted knockouts of genes that would be lethal in a whole-animal knockout, and for interrogation of gene effects within single tissues or cell types (Sauer et al., 1988).

In this study we characterize a mouse strain in which Cre recombinase has been inserted into the *Pou4f2* locus (also referred to as *Brn-3b* or *Brn-3.2*), replacing the *Pou4f2* gene. POU4F2 is a transcription factor necessary for development a large subset of retinal ganglion cells (RGCs). It is essential for RGC differentiation (Erkman et al., 1996, Gan et al., 1996, Xiang et al., 1998, Liu et al., 2000), survival (Gan et al., 1999) and axon path-finding (Wang et al., 2000, Erkman et al., 2000, Badea et al., 2009). We found that this Cre is expressed in all *Pou4f2*-expressing RGCs, and also, over the course of development, becomes expressed in other populations of retinal neurons. We also found the Cre to be expressed in other tissues, including sparsely within visual pathway regions of the brain. In addition to targeting genes in the mouse retina, the $Pou4f2^{Cre}$ line can be used to generate mice in which the number of RGCs is depleted, when the transgene is homozygous (Erkman et al., 1996, Gan et al., 1996). Finally, we found that when $Pou4f2^{Cre}$ is carried by male mice together with a target allele, the Cre targets recombination in the germline. Therefore, a single mouse strain can be used to target recombination in retinal neurons, to deplete RGCs, and to target germline recombination.

My primary contributions to this effort were to characterize the developmental time course of Cre expression in several populations of neurons within the retina, and to

characterize Cre expression within visual regions of the brain. This effort was fundamental to the use of *Pou4f2*^{Cre} in Simmons et al., 2017 (see chapter 1 of this work).

Materials and Methods

Mouse strains and handling: The following mouse strains were used in this study: the cre transgenic mouse *Pou4f2*^{Cre} (courtesy of Dr. Vann Bennett; Duke University) (Fuerst et al., 2012), the Cre-reporter mouse Gt(ROSA)26Sortm9(CAG-tdTomato)Hze (The Jackson Laboratory, Bar Harbor, ME; stock number 007909) (Madisen et al., 2010), and *Dscam* conditional mutant mouse *Dscam*^{tm1Pfu} (referred to as *Dscam*^{FF})(Fuerst et al., 2012). Mouse strains were maintained on a mixed C57Bl6/J, C3H/HeJ and 129 background. All mice carried the wild type allele of *Pde6b*. All protocols were performed in accordance with the University of Idaho Institutional Animal Care and Use Committee. Mice were fed *ad libitum* under 12-hour light/dark cycle.

Tissue preparation: As previously described in chapter 1.

Microscopy: Sections and whole retinas were imaged using an Olympus or Nikon spinning disk confocal microscope or an Olympus Fluoview confocal microscope. Adobe Photoshop was used to crop and rotate images. If brightness or contrast was altered, it was done uniformly across the entire image.

Immunohistochemistry: As previously described in chapter 1.

Antibodies and Stains: *Primary antibodies:* mouse anti-POU4F1/BRN3A (Millipore, Darmstadt, Germany; MAB1585; 1:100); goat anti-POU4F2/BRN3B (Santa Cruz Biotechnology, Santa Cruz, CA; sc-6026; 1:100); rabbit anti-Melanopsin (generous gift from

Ignacio Provencio; 1:10,000); rabbit anti-tyrosine hydroxylase (Millipore; AB152; 1:500); mouse anti-AP2α (Developmental Studies Hybridoma Bank, Trevor J. Williams; 3B5; 1:50); rabbit anti-Calbindin (Swant, Marly, Switzerland; CB-38a; 1:1000); goat anti-Choline Acetyltansferase (Millipore; AB144P; 1:250); rabbit anti-bNOS (Sigma, St. Louis, MO; N7280; 1:5000); mouse anti-PKCα (Santa Cruz Biotechnology, sc-17769; 1:500); rabbit anti-Cone Arrestin (Millipore; AB15282; 1:10,000); mouse anti-Glutamine Synthetase (Millipore; MAB302; 1:1000); mouse anti-calsenilin (Millipore; 05-756; 1:1000); mouse anti-PAX6 (developed by Kawakami, Developmental Studies Hybridoma; 1:500); rabbit anti-Cre (Millipore; 69050-3; 1:500). *Secondary antibodies:* All secondary antibodies were used at 1:1000 (Jackson ImmunoResearch, West Grove, PA). *Stains:* 4′,6-diamidino-2-phenylindole (DAPI) (4083, 1:50,000 from 1 mg/mL stock; Cell Signaling Technology); peanut lectin (PNA) (L21409, L32460; 1:500; Molecular Probes, Eugene, OR, USA).

Results:

Not all of the results of Simmons et al., 2016 are represented in this results section (even though they may be briefly mentioned in the abstract, introduction, and discussion.) This section is intended to represent my contribution to the experiments conducted in Simmons et al. 2016. For full results I encourage the reader to peruse Simmons et al. 2016.

Pou4f2^{Cre} expression determined with activity of *Ai9* Cre reporter

To test the efficiency and location of *Pou4f2*^{Cre} recombination activity, *Pou4f2*^{Cre} mice were crossed to a mouse strain carrying a sensitive and ubiquitously expressed Cre reporter, *Ai9* (Madisen et al., 2010). The Ai9 reporter is driven by the CAG promoter, which is followed by a loxP-flanked transcription termination cassette and red fluorescent protein (RFP). Upon Cre-mediated recombination, the transcription termination cassette is removed, allowing for the transcription of RFP. Cre activity was determined by visualization of RFP in cryo-sections. No visualization of the Ai9 reporter was detected in mice lacking *Pou4f2*^{Cre} .

Pou4f2^{Cre} mediated recombination within the retina.

To test the specificity of *Pou4f2*^{Cre} expression within the retina, *Pou4f2*$^{Cre/+}$ Ai9 retina sections were taken at p35 and immunostained with a panel of cell type specific markers (Table 3.1). Reporter activity was limited to neurons, but was detected in neuron populations not known to express *Pou4f2*. For the majority of markers used in this study only a portion of the cells produced RFP, with the exception of POU4F2, where all counted cells produced RFP (Table 3.1).

Next, *Pou4f2*$^{Cre/+}$ Ai9 retina sections were taken at different ages in order to map out

the developmental time-course at which *Pou4f2^{Cre}* targeted recombination in different cell populations. The proportion of cells producing RFP and positive for specific markers were quantified at P0, P10, P20 and P40 (Figure 3.1). The proportion of cells positive for RFP and PAX6, ChAT and calsenilin increased incrementally from P0 to P40, while POU4F2 positive cells were all targeted starting from P0, the earliest time point sampled (Figure 3.1 A-I). Immunohistochemistry was then used to detect the location of Cre protein (Figure 3.1 J-M). Cre protein was observed within the neurites and nuclei of cells in which recombination occurred (Figure 3.1 J), while staining was absent in retina sections taken from mice lacking Cre (Figure 3.1 K). Cre protein was observed within the nuclei and neurites of subsets of ganglion cells and horizontal cells, confirmed by co-staining with POU4F2 and PAX6 (not shown), but was absent from the nuclei of amacrine and bipolar cells at P10 (Figure 3.1 L, L'). Cre protein was observed within the nuclei of cells in the RGL and INL by P40, consistent with reporter activation (Figure 3.1 M and M'). Late activity of *Pou4f2^{Cre}* was also effective in targeting constructs other than the highly sensitive *Ai9* reporter. A conditional allele of Down syndrome cell adhesion molecule *(Dscam)* was used to demonstrate this activity, which is evidenced by the accumulation of DSCAM protein with the cells bodies of targeted cells (de Andrade et al., 2014). *Dscam* targeting was observed in ganglion cells and amacrine cells early during development, and later (~P45) in bipolar cells (Figure 3.1 N).

Pou4f2^{Cre} activity within the brain.

Pou4f2$^{Cre/+}$ Ai9 brains brain cryosections were imaged to test the specificity of *Pou4f2^{Cre}* expression within the brain. RFP was observed in many regions of the brain (Figure 3.2). The expression of RFP was observed in retinal ganglion cell axons projecting throughout

the brain, but was also found within neural cell bodies and their neurites in other regions of the brain, including visual centers, consistent with previous studies (Badea et al., 2009, Sajgo et al., 2014).

Discussion

This study characterized a *Pou4f2*^{Cre} transgenic mouse line, in which Cre recombinase is driven by the *Pou4f2* promoter. We find 1) *Pou4f2*^{Cre} is expressed in all Pou4f2 expressing RGCs and becomes expressed in other of retinal neuron populations over development. 2) *Pou4f2*^{Cre} is expressed sparsely within visual pathway regions of the brain, as well as within other body tissues 3) *Pou4f2*^{Cre} functions as a loss-of-function of the *Pou4f2* gene and, as one would predict given its important role in RGC development, homozgosing *Pou4f2*^{Cre} leads to RGC depletion. 4) When *Pou4f2*^{Cre} is carried by male mice together with a target allele, the Cre targets recombination in the germline.

Our finding that timing of *Pou4f2*^{Cre} mediated recombination within the retina depends on the cell type gave us a reproducible method to target amacrine and bipolar cells late in development. In Chapter 1 of this thesis we use this to target *Dscam* in Type 4 OFF cone bipolar cells (BC4s) after developmental cell death and dendrite outgrowth, demonstrating that growth plasticity in these cells in restrained by *Dscam* and can be re-initiated after *Dscam* deletion. Thus, characterizing the developmental time-course of *Pou4f2*^{Cre} in different populations of neurons was a vital preliminary to that finding in Simmons et al., 2017 (see chapter 1). The expression of Cre from the *Pou4f2* locus differs from immunohistological studies in which RGCs are the primary cell type of the retina expressing *Pou4f2*^{Cre} and related proteins (Badea et al., 2009). In Simmons et al. 2016 we speculate on why this may be the case.

We think our finding of sparse recombination in other tissues – visual regions of the brain, neurons of the enteric nervous system, photoreceptors – may also prove useful to researchers wishing to perform genetic manipulations confined to small number of cell in

these regions/populations.

In conclusion, this study characterizes a transgenic *Pou4f2* knock-in Cre recombinase transgenic mouse line. This line can be used to deplete RGC number, to target germline recombination and to target recombination in retinal neurons while sparing Müller glia and most photoreceptors. I encourage readers of this thesis chapter to consult Simmons et al., 2016 if they are curious about other features of this research

References

Badea TC, Cahill H, Ecker J, Hattar S, Nathans J. Distinct roles of transcription factors brn3a and brn3b in controlling the development, morphology, and function of retinal ganglion cells. Neuron. 2009;61(6):852-64.

de Andrade GB, Long SS, Fleming H, Li W, Fuerst PG. DSCAM localization and function at the mouse cone synapse. The Journal of comparative neurology. 2014;522(11):2609-33.

Erkman L, McEvilly RJ, Luo L, Ryan AK, Hooshmand F, O'Connell SM, Keithley EM, Rapaport DH, Ryan AF, Rosenfeld MG. Role of transcription factors Brn-3.1 and Brn-3.2 in auditory and visual system development. Nature. 1996;381(6583):603-6.

Erkman L, Yates PA, McLaughlin T, McEvilly RJ, Whisenhunt T, O'Connell SM, Krones AI, Kirby MA, Rapaport DH, Bermingham JR, O'Leary DD, Rosenfeld MG. A POU domain transcription factor-dependent program regulates axon pathfinding in the vertebrate visual system. Neuron. 2000;28(3):779-92.

Fuerst PG, Bruce F, Rounds RP, Erskine L, Burgess RW. Cell autonomy of DSCAM function in retinal development. Developmental biology. 2012;361(2):326-37.

Gan L, Xiang M, Zhou L, Wagner DS, Klein WH, Nathans J. POU domain factor Brn-3b is required for the development of a large set of retinal ganglion cells. Proceedings of the

National Academy of Sciences of the United States of America. 1996;93(9):3920-5.

Gan L, Wang SW, Huang Z, Klein WH. POU domain factor Brn-3b is essential for retinal ganglion cell differentiation and survival but not for initial cell fate specification. Developmental biology. 1999;210(2):469-80.

Liu W, Khare SL, Liang X, Peters MA, Liu X, Cepko CL, Xiang M. All Brn3 genes can promote retinal ganglion cell differentiation in the chick. Development. 2000;127(15):3237-47.

Madisen L, Zwingman TA, Sunkin SM, Oh SW, Zariwala HA, Gu H, Ng LL, Palmiter RD, Hawrylycz MJ, Jones AR, Lein ES, Zeng H. A robust and high-throughput Cre reporting and characterization system for the whole mouse brain. Nature neuroscience. 2010;13(1):133-40.

Sajgo S, Ghinia MG, Shi M, Liu P, Dong L, Parmhans N, Popescu O, Badea TC. Dre - Cre sequential recombination provides new tools for retinal ganglion cell labeling and manipulation in mice. PloS one. 2014;9(3):e91435.

Sauer B, Henderson N. Site-specific DNA recombination in mammalian cells by the Cre recombinase of bacteriophage P1. Proceedings of the National Academy of Sciences of the United States of America. 1988;85(14):5166-70.

Simmons AB, Bloomsburg SJ, Billingslea SA, Merrill MM, Li S, Thomas MW, Fuerst PG.

Pou4f2 knock-in Cre mouse: A multifaceted genetic tool for vision researchers. Mol Vis. 2016 Jun 23;22:705-17

Wang SW, Gan L, Martin SE, Klein WH. Abnormal polarization and axon outgrowth in retinal ganglion cells lacking the POU-domain transcription factor Brn-3b. Molecular and cellular neurosciences. 2000;16(2):141-56.

Xiang M. Requirement for Brn-3b in early differentiation of postmitotic retinal ganglion cell precursors. Developmental biology. 1998;197(2):155-69.

General conclusions

These experiments were conducted to contribute to understanding of the retina and its organization. Such and understanding is important because vision is our primary sense and we want to know how it works and how diseases and injuries within it can be treated. It is also important because it is made of the same stuff as the brain, so we can study the brain by proxy with the retina, which is by far the most accessible part of the central nervous system.

We have, in fact, contributed. We have shown that DSCAM and the homotypic avoidance that it mediates is important not only to organization during development but to plasticity in adulthood. Homotypic avoidance, something that we think of as a developmental thing, is active in adulthood. Along this same line, we showed that BC4s are ordinarily plastic for much longer than was previously assumed.

We have also shown that bipolar cells limit their own growth to make their axon and dendrite arbors match in size, and ensure that neither is covering territory that the other is not. We think that this is a design principle separate from homotypic avoidance, but which operates alongside it to ensure the accuracy of spatial information encoded by BCs.

Along the way, we have developed tools that we anticipate will be useful to other researchers. We characterized *Pou4f2-cre* and used to in BC4s as a means to control timing of *Dscam* knockout, in which role it was extremely useful. We expect that other researchers will find other uses for *Pou4f2-cre*, but our use of it provides an example of one of the useful things we found about our model system for most of these experiments: the mouse BC4.

Many extremely useful elements came together in mouse BC4s. The tiling mosaic of BC4s organization provides a system with potential for screening and scoring changes in

organization and plasticity. The measurements and quantifications we were able to perform depended on the existence of this mode of organization. In this system we had ready-made tools for doing genetic manipulations. The genetic manipulation we performed, *Dscam* knockout, was useful for my studies of growth limitation because it knocked out homotypic avoidance. We also had tools for density manipulation: the natural variation in BC4 density noted in chapter 2, increase in density caused by *Bax* knockout (not represented in this work), and, for future work, diphtheria-toxin-based depletion. Alongside the tools for genetic manipulations, we had relatively specific transgenic fluorescent markers and a cell specific immunological marker. These tools that allowed us to do high quality imaging, and the high quality imaging enabled the extensive and precise measurements that our studies were dependent on.

We did a lot of measuring. Coming up with measurements is important in science. I think that the real strength of many of the measurements that we developed is that they looked at the feature of interest holistically and in context. To look at loss of tiling you have to look at a cell and its neighbor. To look at a link between dendrite arbor size and axon arbor size you need to look at dendrites and axons. To look at a community feature like the region that the community leaves un-sampled, you need to measure whole communities. And if you want to look at how a single cell within such a community behaves, you need a system that allows you to measure both the community and the individual cell. There is a place for looking at a particular phenomenon in isolation. But a lot of things can only be understood in a bigger context, so you have to measure stuff in context. I think we tried to do that. Obviously we're not the only ones.

Transgene	Name	Properties	Promotor	Usage	Notes
Dscam^{tm1Pfu}	*Dscam*^{FF}	Exon 27 of *Dscam* is flanked by LoxP	N/A	Targetted deletion of *Dscam* by transgenic Cre	flanked by loxP = "floxed"
Gt(ROSA)26 Sortm9(CAG-tdTomato)Hze	*Ai9*	tdTomato Cre reporter in rosa26 locus	CAG synthetic high expression promotor	Cre reporter	
Pou4f2-cre	*Pou4f2-cre*	Transgenic cre, inserted into *Pou4f2* gene	Pou4f2	Targetting deletion of floxed genes	Pou4f2 is a transcription factor expressed in a large set of RGC
Tg(Htr2a-cre)KM207G sat	*5-Htr2a-cre*	Transgenic cre, inserted immediately upstream of start ATG of *5-Htr2a* gene	5-Htr2a	Targetting deletion of floxed genes	5-HT, or 5-hydroxytryptamine, is also called serotonin. 5-HT receptor 2a is expressed in BC4
5-Htr2a-EGFP	*5-Htr2a-GFP*	Transgenic GFP inserted immediately upstream of start ATG of *5-Htr2a* gene	5-Htr2a	Transgenic GFP	See above
	Dscam$^{Non\text{-}targetted}$	An individual BC4 in *Dscam*^{FF} ; *5-HTR2a-cre* retina in which cre is not expressed	N/A	a cell with WT *Dscam* in a population of cells that, overall, lacks *Dscam*	~80% of BC4s in *Dscam*^{FF} ; *5-HTR2a-cre* retina express cre
	Dscam^{Targetted}	An individual BC4 in *Dscam*^{FF} ; *5-HTR2a-cre* retina in which cre is expressed	N/A	these cells lack *Dscam*	See above

Table 1.1 Transgenes. This table summarizes the transgenes used in this paper, their purpose, and the names they are referred to by. This table is comprehensive for chapters 1, 2 and 3.

Table 3.1: Retinal Cell Types Expressing *Pou4f2*^{Cre}		
Marker	**Population**	**Cre+ (%)**
POU4F2 (BRN3B)	RGCs	100
POU4F1 (BRN3A)	RGCs	86
Melanopsin	RGCs	79
AP2α	ACs	44
Calbindin	ACs	60
	HCs	100
ChAT	Cholinergic ACs	97
bNOS	bNOS ACs	38
TH	Dopaminergic ACs	50
PKCα	Rod BCs	0
Cone Arrestin	Cones	2
GS	Müller Glia	0*
IBA-1	Microglia	0
GFAP	Astroctyes	0
GS iso B4	Blood Vessels	0

Table 3.1. Retinal Cell Types Expressing *Pou4f2*^{Cre}. Immunohistochemistry was performed on *Pou4f2*$^{Cre/+}$ Ai9 retinas to determine which cells types within the retina express *Pou4f2*^{Cre}. This table summaries Figure 3 and 4 and contains markers not shown (IBA-1, GFAP, GS isolection-B4). *1 out of 34 mice contained sparsely labeled Müller glia, where columns of cells expressed tdTomato. Abbreviations: ACs—amacrine cells, BCs—rod bipolar cells, HCs—horizontal cells, RGCs—retinal ganglion cells, TH—tyrosine hydroxylase, PKC—protein kinase C, GS—glutamine synthetase.

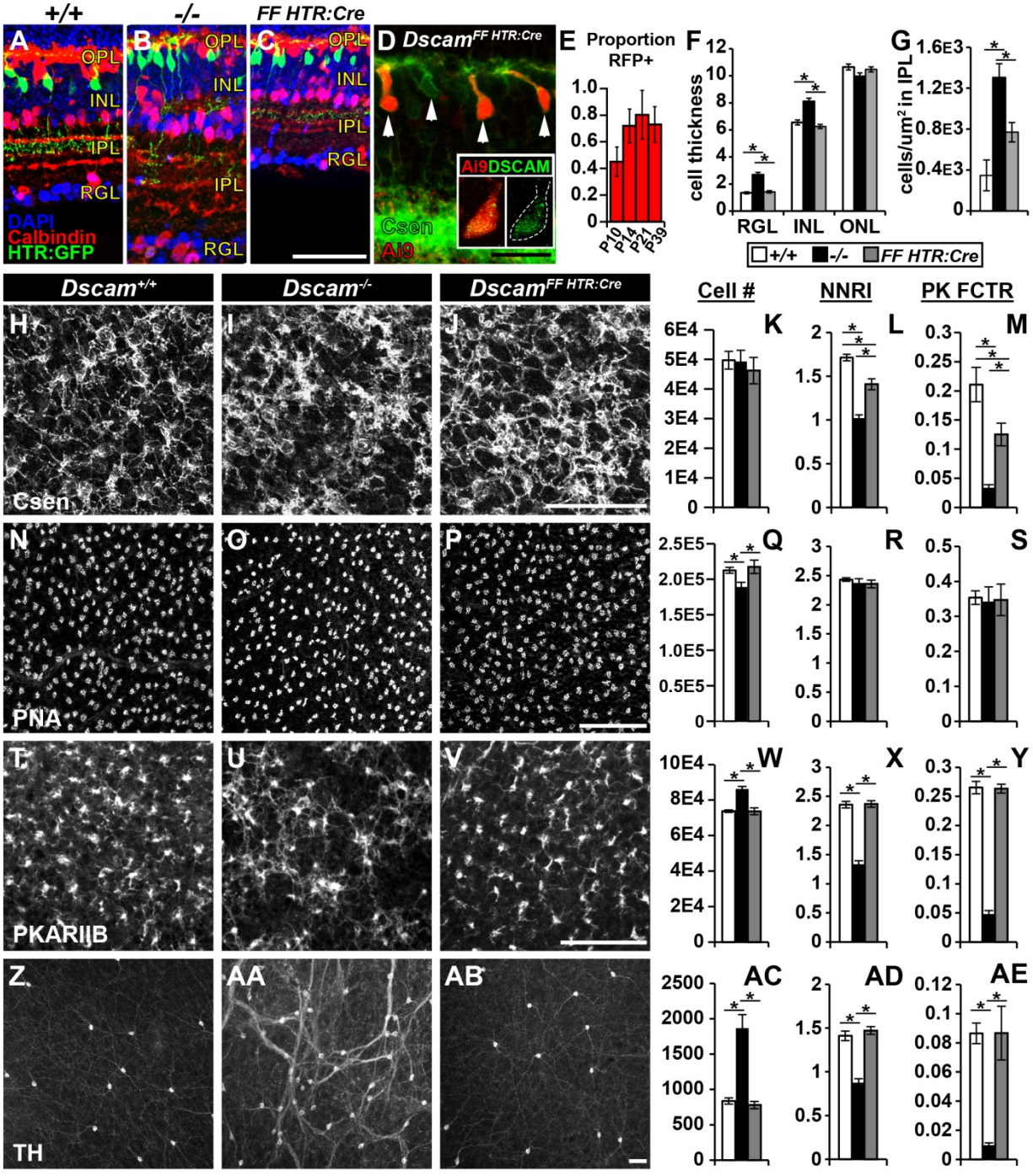

Figure 1.1. Conditional targeting of *Dscam* with *HTR:Cre*. (A-C) Cryo-sections of retina stained with DAPI, calbindin and *HTR:GFP*. (A) *Dscam*$^{+/+}$ retina, organization of the retina in to alternating nuclear and synaptic layers. Lamination of the IPL is organized into sublamina, illustrated by calbindin staining and lamination of BC4 axons. (B) *Dscam*$^{-/-}$ retina,

highly disorganized retinal layers due to defects in neural organization and cell death. (C) *Dscam*$^{FF\ HTR:Cre}$ retina, integrity of the retinal layers and lamination of the IPL is maintained. (D-E) *HTR:Cre* targeting efficiency of the *Ai9* reporter and *Dscam* floxed alleles. By P14, *HTR:Cre* targets ~75% of BC4s, evidenced by *Ai9* expression and accumulation of DSCAM protein in the cytosol after the transmembrane domain is removed by cre-mediated recombination. (F) Quantification of retinal thickness in each nuclear layer. (G) Quantification of displaced cells in the IPL. Significant increases in cellularity is observed in the *Dscam*$^{-/-}$ retina compared to *Dscam*$^{+/+}$ or *Dscam*$^{FF\ HTR:Cre}$ retinas. (H-AE) Cell number, NNRI and Packing factors were quantified and compared in whole-mount retinas at 1m of age in *Dscam*$^{+/+}$, *Dscam*$^{-/-}$, and *Dscam*$^{FF\ HTR:Cre}$ retinas for multiple cell types known to require DSCAM for proper cell death and/or dendrite arborization. Cones do not require DSCAM, but were included in the analysis because they are the main presynaptic input for BC4s. (H-M) BC4s, no significant changes in cell number were detected. Significant reductions in both the NNRI and packing factor were detected when comparing *Dscam*$^{+/+}$ to *Dscam*$^{-/-}$ and *Dscam*$^{FF\ HTR:Cre}$, and when comparing *Dscam*$^{-/-}$ to *Dscam*$^{FF\ HTR:Cre}$. (N-S) Cones, a significant reduction in cones was detected when comparing *Dscam*$^{-/-}$ to *Dscam*$^{+/+}$ or *Dscam*$^{FF\ HTR:Cre}$ retinas. No significant changes to NNRI or packing factor were detected. (T-Y) BC3bs, significant increases in cell number was detected when comparing *Dscam*$^{-/-}$ to *Dscam*$^{+/+}$ or *Dscam*$^{FF\ HTR:Cre}$ retinas. Significant reductions in NNRI and packing factor were detected when comparing *Dscam*$^{-/-}$ to *Dscam*$^{+/+}$ or *Dscam*$^{FF\ HTR:Cre}$ retinas. (Z-AE) DACs, significant increases in cell number was detected when comparing *Dscam*$^{-/-}$ to *Dscam*$^{+/+}$ or *Dscam*$^{FF\ HTR:Cre}$ retinas. Significant reductions in NNRI and packing factor were detected when comparing *Dscam*$^{-/-}$ to *Dscam*$^{+/+}$ or *Dscam*$^{FF\ HTR:Cre}$ retinas. Scale bars = 50μm. Abbreviations:

ONL, outer nuclear layer; OPL, outer plexiform layer; INL, inner nuclear layer; IPL, inner plexiform layer; RGL, retinal ganglion cell layer; RFP, red fluorescent protein; NNRI, nearest neighbor regularity index; PK FCTR, packing factor.

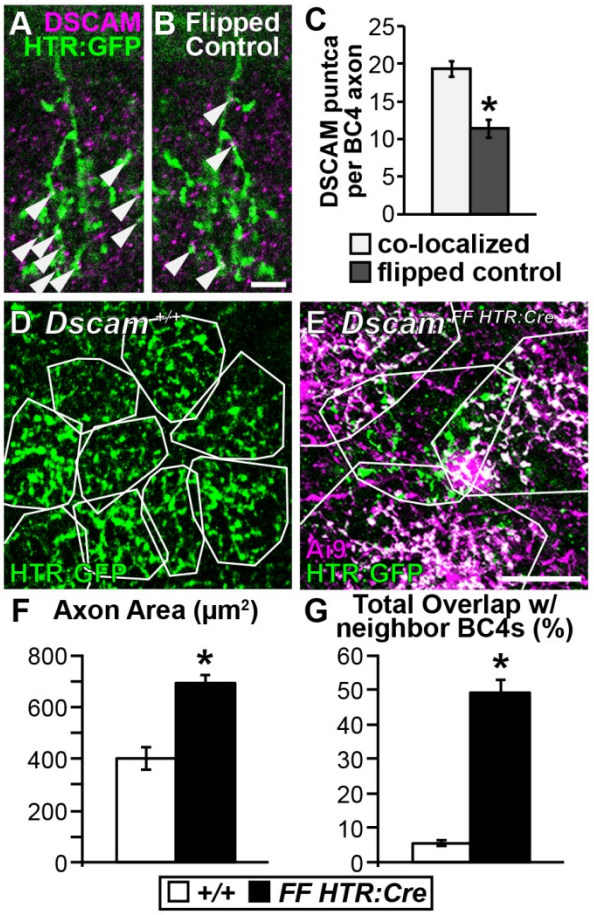

Figure 1.2. *Dscam* is necessary and sufficient to establish and maintain BC4 axon tiling. (A-C) Co-localization of DSCAM protein with BC4 axons. Of note, this analysis was performed in serial z-stack images, shown here is a single confocal plane from an analyzed stack. (A-B) Cryo-sections of retina stained with anti-DSCAM and *HTR:GFP* to determine co-localization. (A) Image showing DSCAM/BC4 axon co-localization. (B) Axon channel flipped about the horizontal axis as a control for incidental co-localization. Arrowheads point to co-localized DSCAM puncta on BC4 axons. (C) Quantification of DSCAM puncta co-localization per BC4 axon. A significant increase in DSCAM puncta was detected when comparing the original images to the flipped controls. (D-E) Three-month flat-mount retina, BC4s are labeled genetically (*HTR:Cre x Ai9* and *HTR:GFP or HTR:GFP* only). (D) $Dscam^{+/+}$, BC4 axons outlined in white to visualize tiling. (E) $Dscam^{FF\ HTR:Cre}$, axons outline

in white. Only the green axon is a single axon. The others outlined are multiple BC4 axons bundled together. Green axon is a *Dscam*^{NonTar} BC4. Axons invade each others territory when one or both lack DSCAM. (F-G) Quantifications of axon area (F) and total overlap with neighboring BC4 axons (G). *Dscam*^{NonTar} BC4 axons, become significantly larger and overlap significantly more with neighboring *Dscam*^{Tar} BC4 axons when compared to *Dscam*$^{+/+}$ BC4 axons. Scale bar in B = 5μm; E = 20μm.

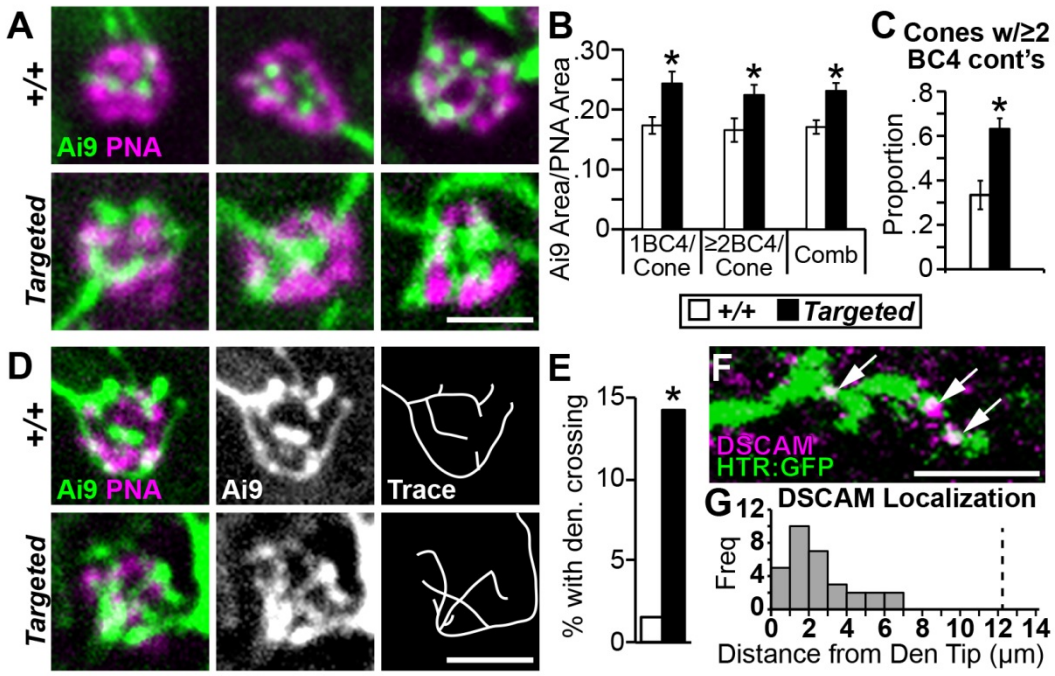

Figure 1.3. *Dscam* is necessary and sufficient for iso-neuronal avoidance at the cone synapse in BC4s. (A) High magnification images of single BC4s making contact with cones at three months of age in whole-mount retinas. *Dscam*$^{+/+}$ BC4s make connections with cones that are highly organized and vary in their amount of contacts at a single cone. *Dscam*^{Tar} BC4s make connections with cones that are disorganized and their dendrites clump together. (B) Quantification of total amount of BC4 dendrites localized within PNA area. Significant increases in coverage were observed in *Dscam*^{Tar} BC4s compared to *Dscam*$^{+/+}$ BC4s, regardless if the cones were contacted by 1BC4 or ≥2BC4s. No significant differences were detected in PNA area (data not shown). (C) Quantification of cones contacted by two or more BC4s. A significant increase was observed in *Dscam*$^{FF\ HTR:Cre}$ compared to *Dscam*$^{+/+}$. (D) High magnification images of single BC4s making contact with cones at three-months of age. *Dscam*$^{+/+}$ BC4s dendrites do not cross. *Dscam*^{Tar} BC4s dendrites frequently cross. (E) Quantification of observed dendrite crossing at the cone. Statistically more dendrites cross in *Dscam*^{Tar} BC4s compared to *Dscam*$^{+/+}$ BC4s. (F) High magnification image of DSCAM co-

localization with *Dscam*$^{+/+}$ BC4 dendrites in cryo-sections. Arrows point to co-localization. (G) Quantification of the distance DSCAM puncta is localized from the nearest BC4 dendritic tip. DSCAM was observed as far away as 7μm from the dendrite tip. The vertical dotted line at 12.2μm represents the average dendrite length from dendrite terminal to cell body. Scale bars = 3μm. Abbreviations: comb, combined; cont's, contacts; freq, frequency.

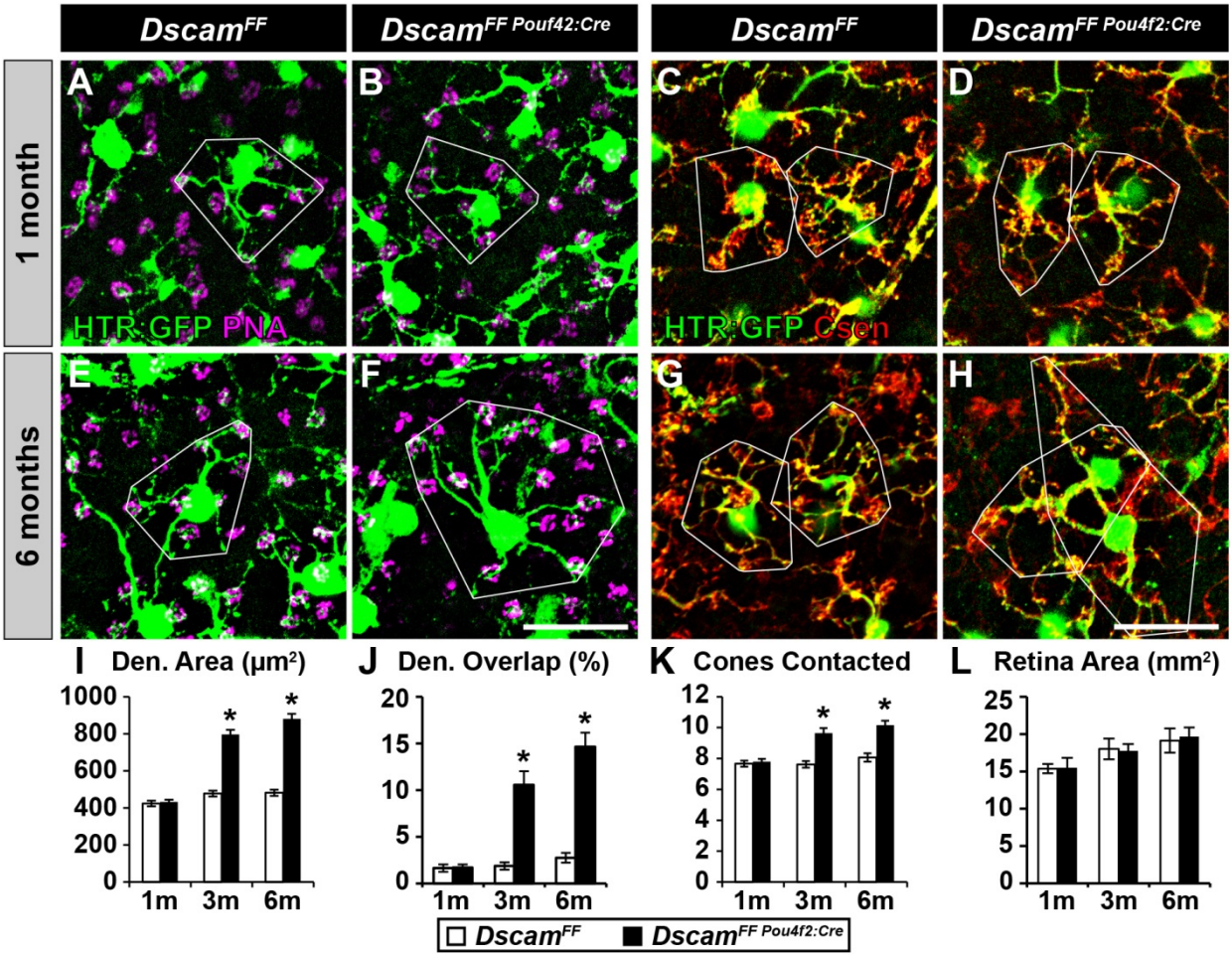

Figure 1.4. *Dscam* is necessary and sufficient to inhibit BC4 dendritic plasticity in the adult retina. Late deletion of the *Dscam* floxed allele was accomplished with *Pou4f2:Cre*, which effectively recombines *Dscam* by P45(cite). *Dscam*^{FF} BC4s were compared to *Dscam*$^{FF\ Pou4f2:Cre}$ BC4s before *Pou4f2:Cre* mediated recombination of *Dscam* occurs, 1m (A-B and E-F), and then compared at two more time-points after recombination occurs, 3m and 6m (C-D and G-H). (A-D) Whole-mount retinas with BC4s labeled with *HTR:GFP* and stained with PNA to visualize cones at 1m (A-B) and 6m (C-D). Dendrite area of a single cell is mapped in white. *Dscam*$^{FF\ Pou4f2:Cre}$ BC4s become dramatically larger and contact more cones after recombination compared to *Dscam*^{FF} BC4s. (E-H) Whole-mount retinas with BC4s labeled with *HTR:GFP* and stained with anti-calsenilin antibody at 1m (E-F) and 6m (G-H).

Neighboring BC4s mapped in white. *Dscam*$^{FF\ Pou4f2:Cre}$ BC4s begin to invade neighboring BC4's territory after recombination, while tiling remains intact in *Dscam*^{FF} BC4s at all time-points. (I-K) Quantifications of dendrite area (I), cones contacted (J), and dendrite overlap (K). *Dscam*^{FF} BC4s and *Dscam*$^{FF\ Pou4f2:Cre}$ BC4s are not statistically different for any of these measures at 1m of age. However, *Dscam*$^{FF\ Pou4f2:Cre}$ BC4s become statistically greater for all of these measurements at 3m and 6m. (L) Quantification of total retina area. No statistical differences were observed between *Dscam*^{FF} and *Dscam*$^{FF\ Pou4f2}$ retinas. Scale bars = 20μm.

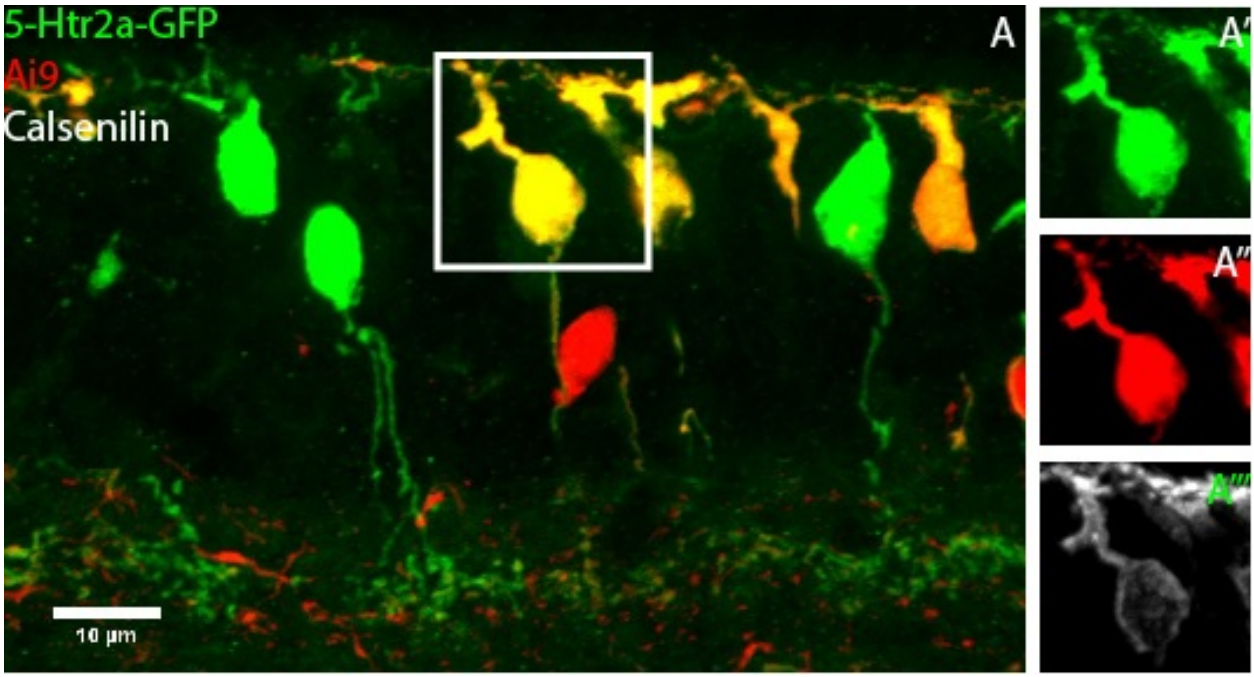

Figure 2.1. Markers used for imaging BC4s. A, The fluorescent transgenes 5-Htr-GFP and Ai9 reporter after activation by 5-Htr-cre, and the BC4 specific anti-calsenilin antibody. For clarity, calsenilin is omitted from large panel A. **A',** Inset showing GFP only. **A'',** Inset showing Ai9 only. **A''',** Inset showing anti-calsenilin only.

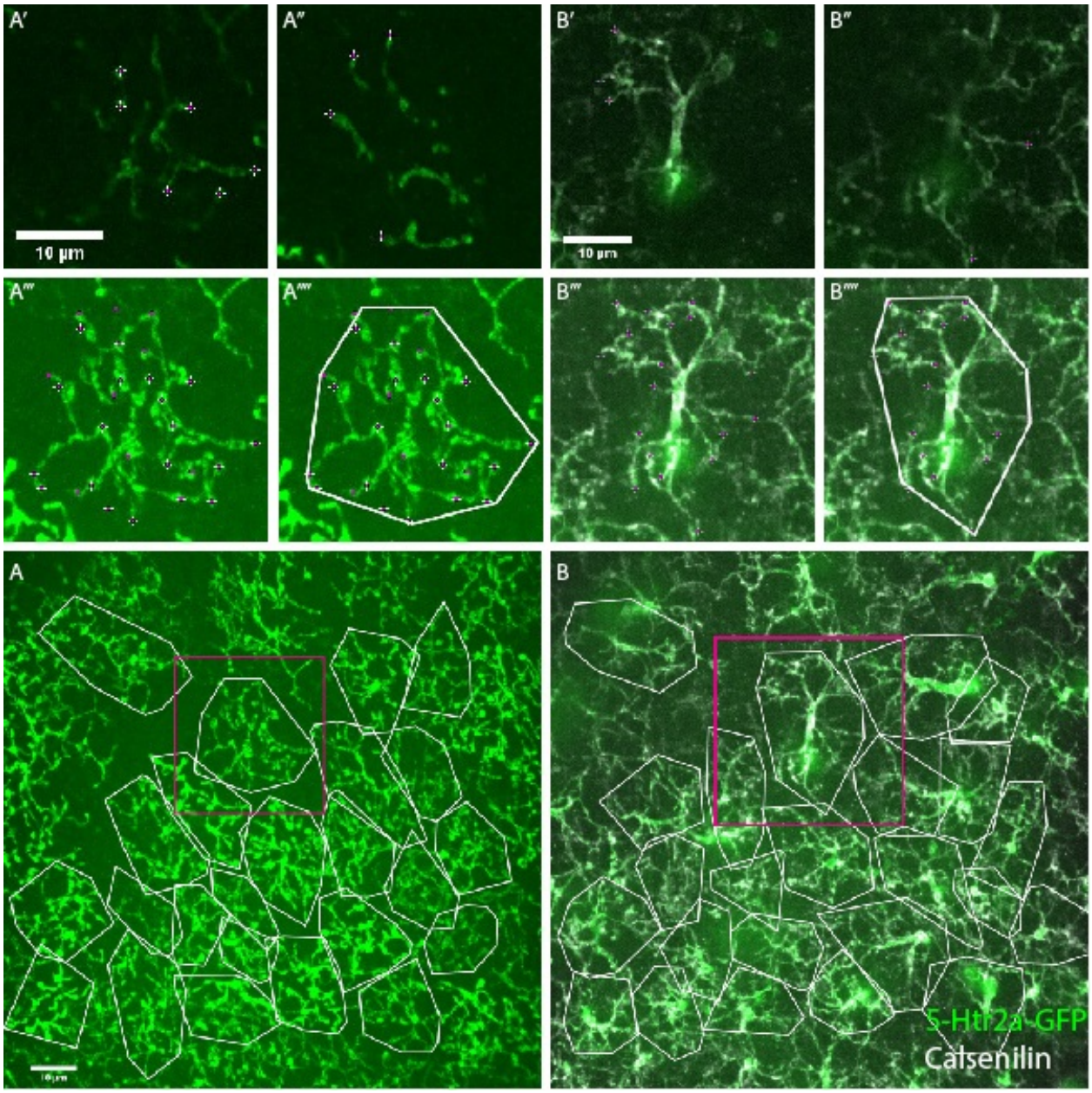

Figure 2.2. Reconstruction of BC4 axon and dendrite arbors. A, Full field of reconstructed axon arbors. **B,** Full field of reconstructed dendrite arbors. **A'-A'''' ''** demonstrate process of reconstructing single axon arbor. **B'-B'''' ''** demonstrate process of reconstructing single dendrite arbor

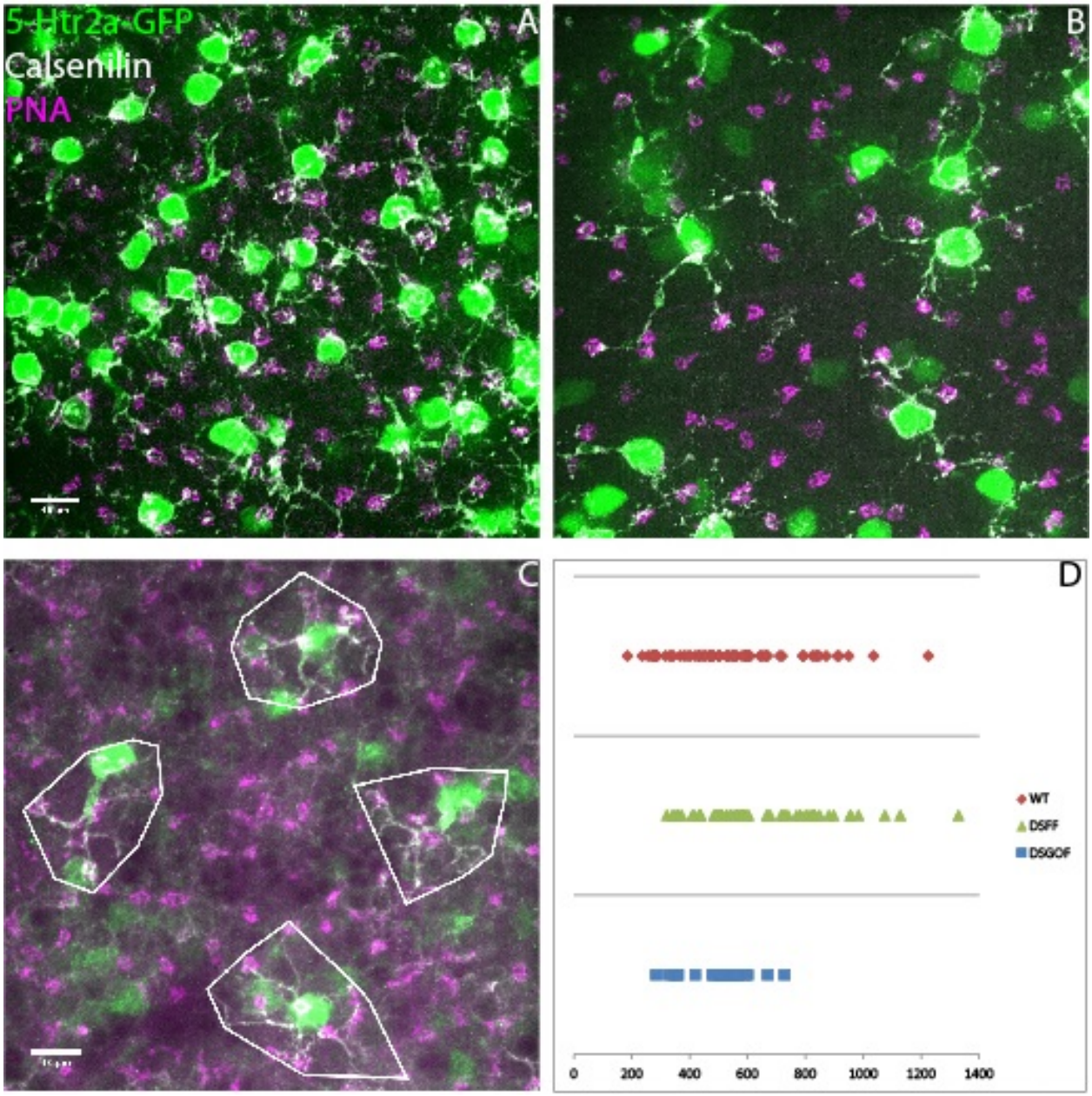

Figure 2.3. BC4 Dendrites, with 5-Htr-GFP, calsenilin, and PNA. **A,** WT BC4 dendrites, central retina. **B,** WT BC4 dendrites, peripheral retina. **C,** DscamGOF dendrites, middle retina. **D,** Distribution of dendrite arbor sizes in WT, DscamFF, and DscamGOF retinas.

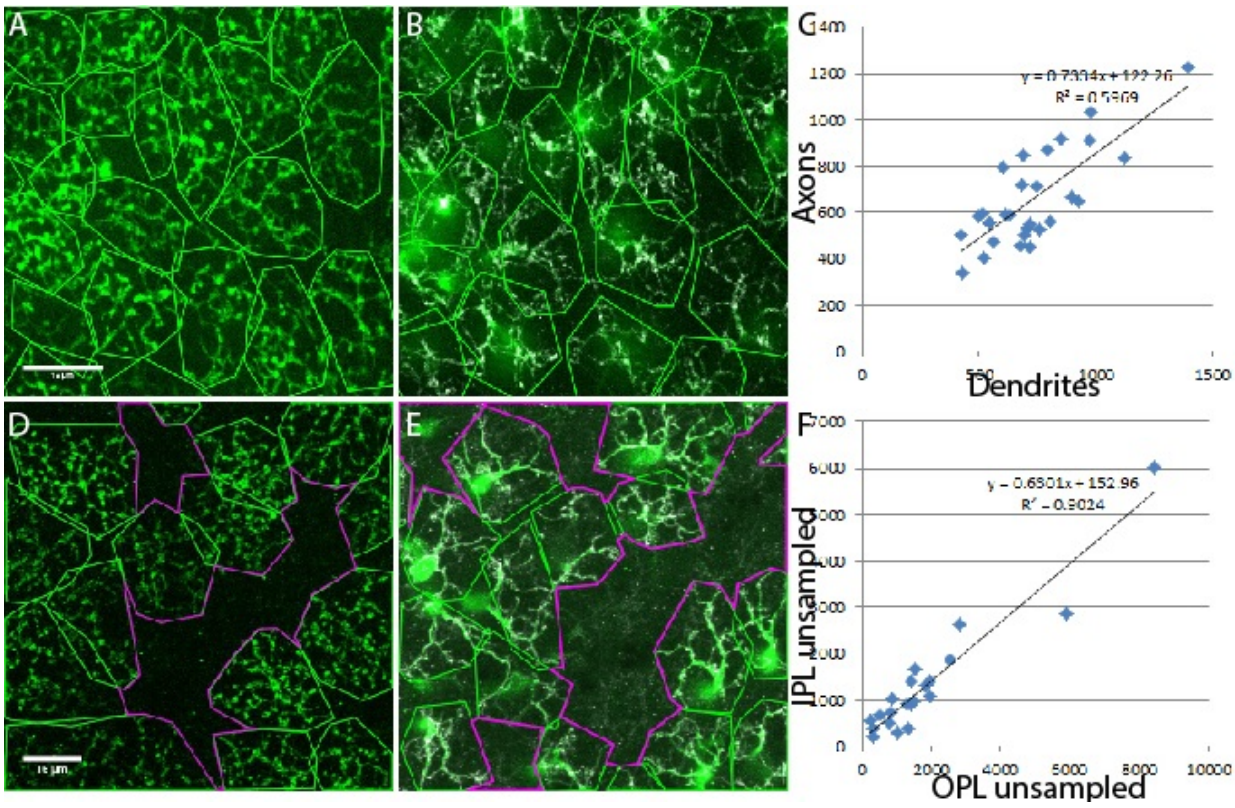

Figure 2.4. Correlation of dendrite arbor to axon arbor size and un-sampled space in the OPL and IPL. A, A field of reconstructed axons. **B,** A field of reconstructed dendrites. **C,** Dendrite arbor area plotted against axon arbor area for the same cell, regression line of same. 67 data points from 7 retinas. **D,** Unsampled IPL regions and reconstructed axons. **E,** Unsampled OPL regions and reconstructed dendrites. **F,** Unsampled OPL area plotted against unsampled IPL area, regression of same. 21 data points from 4 retinas.

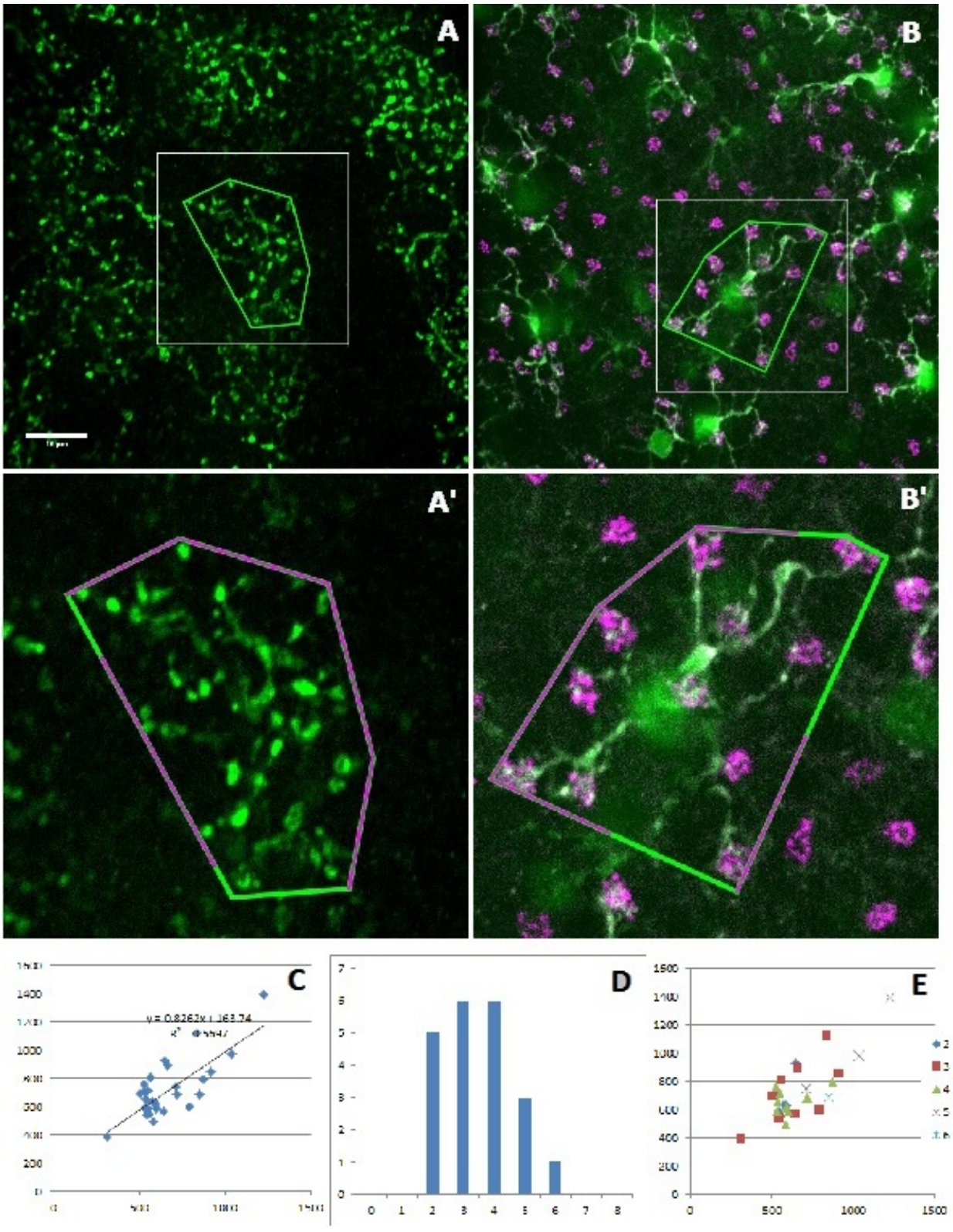

Figure 2.5. Isolated BC4s. A, Axon arbor of an isolated BC4. **B,** Dendrite arbor of a BC4.

A', Demonstration of isolation scoring procedure. **B',** Demonstration of isolation scoring procedure. **C,** Regression analysis of dendrite arbor size vs. axon arbor size for BC4s with isolation score ≥2. 21 data points from 4 retinas. **D,** Histogram representing isolation scores of cells used in analysis. **E,** Cells of each score grouping were plotted together. It can be seen that the same trend line fits all the data.

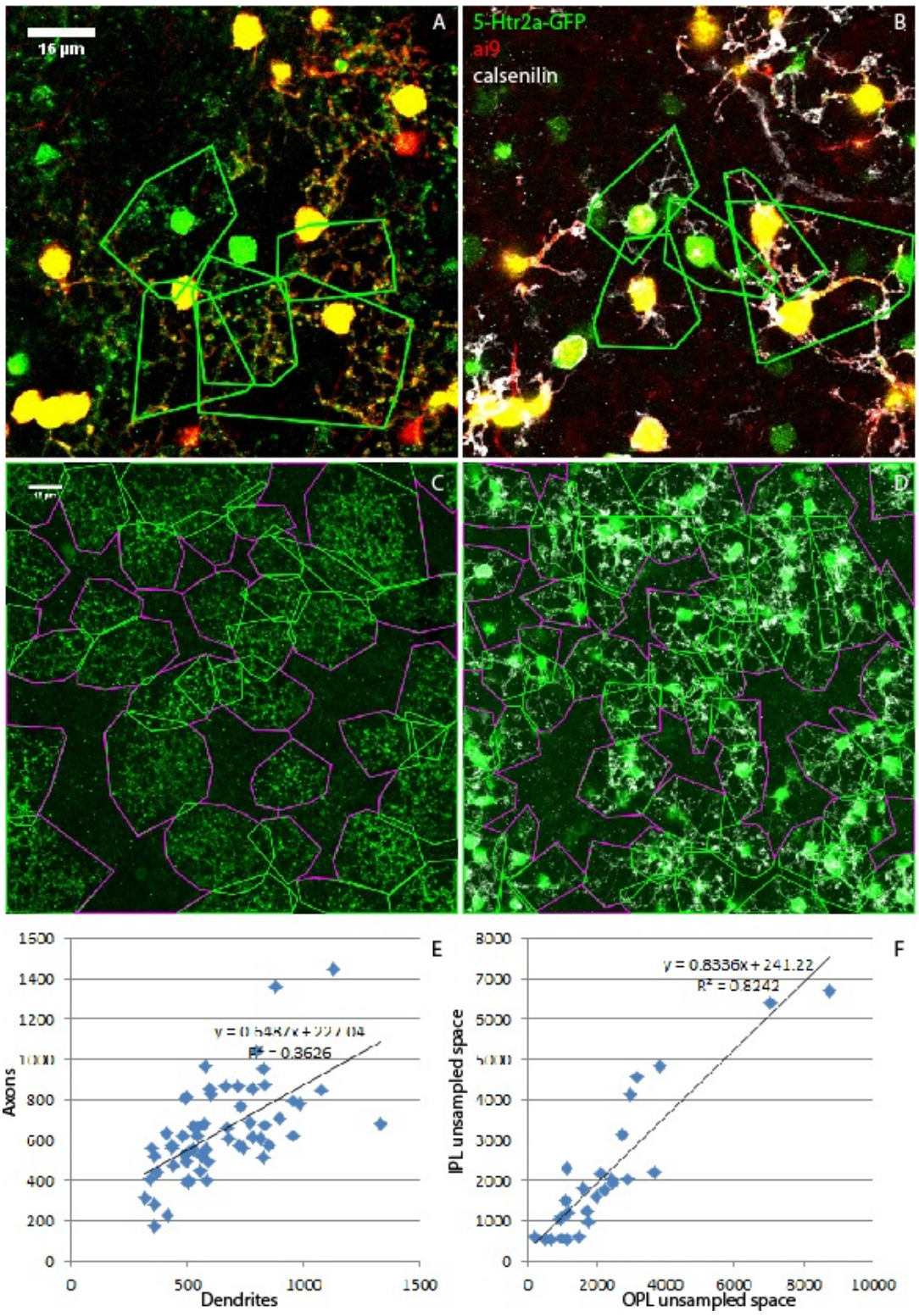

Figure 2.6. Dendrite axon correlation and un-sampled OPL and IPL in DscamFF retinas. A, Non-targeted (green) and targeted (yellow) axons in DscamFF retina. **B,** Dendrites

in DscamFF retina. **C,** Un-sampled IPL. **D,** Unsampled OPL E. Regression of dendrite arbor size vs axon arbor size in DscamFF retina. **F,** regression of un-sampled OPL vs un-sampled IPL in DscamFF retina. In **E** and **F**, ai9 is omitted for clarity.

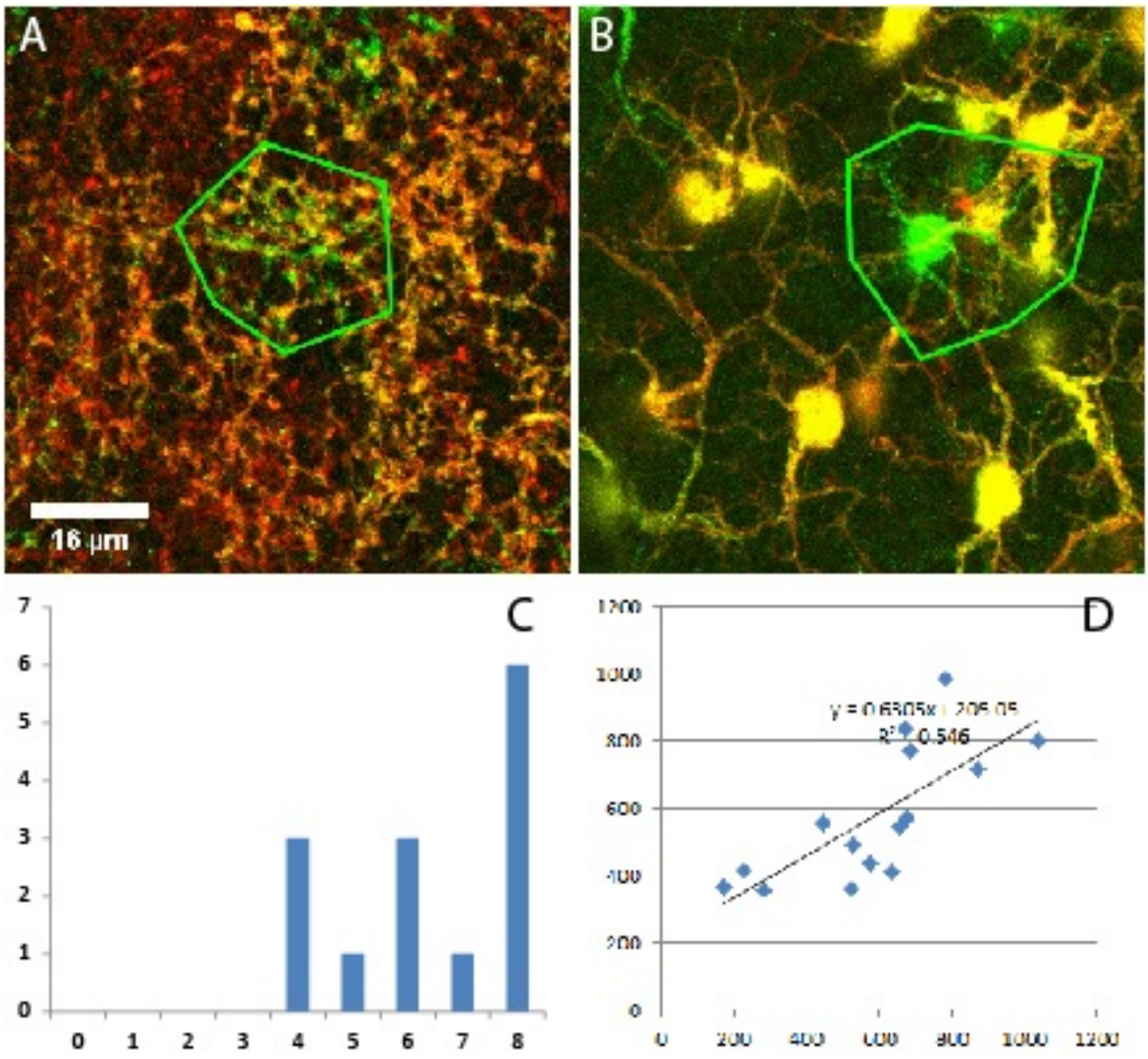

Figure 2.7. "Functionally isolated" non-targeted cells within DscamFF retina. A, non-targeted axons surrounded by targeted axons. **B,** non-targeted dendrites surrounded by targeted dendrites. **C,** Isolation scores of analyzes cells. **D,** regression analysis of functionally isolated cells.

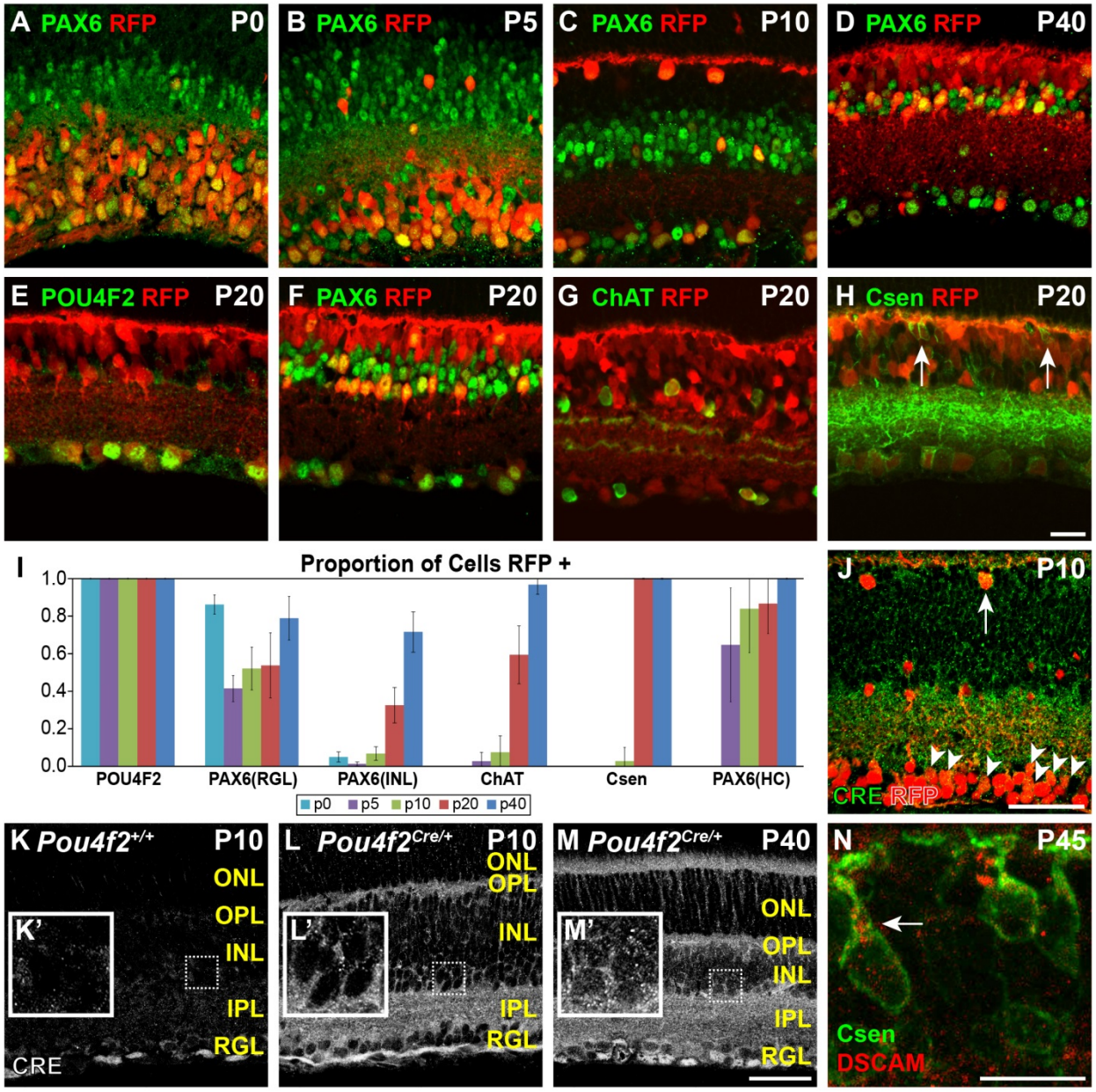

Figure 3.1. Developmental time-course of *Pou4f2*^{Cre} activity within the retina. A developmental time-course of Cre targeting within the retina was performed by immunostaining cryo-sections of retina with neural markers (PAX6, POU4F2, ChAT and Calsenilin). The proportions of reporter positive cells for each of the markers at P0, P5, P10, P20 and P40 were quantified. Progression in the proportion of cells targeted by *Pou4f2*^{Cre}

increased in all of the markers over developmental time, except for POU4F2 positive cells, which were 100% targeted starting from P0. **A-D,** developmental time-course of PAX6 except P20. **E-H,** representative images of all the markers at P20. **I,** Graph illustrating the proportion of cells positive for the Ai9 reporter over time. PAX6-positive cells were subdivided into cells found within the RGL, INL and HCs in the outer INL. Calsenilin (Csen) was used to label Type 4 bipolar cells and bipolar cells were the only quantified cell type reported for this stain. **J**-**M**, Cre protein staining. **J**, Cre was detected within cell bodies and neurites of cells in the RGL (arrowheads) and horizontal cells (arrow). **K,** Cre negative control. Cre protein was not observed. **L,** Cre was detected within the nuclei and neurites of cells within the RGL but was absent from most nuclei within the INL at postnatal day 10 (P10) (L'). **M,** Cre was detected within the nuclei of cells in the RGL and INL, consistent with reporter activation. **M',** Inset showing Cre within cells of the INL. **N,** *Pou4f2*^{Cre} effectively targets a conditional allele of *Dscam* at P45 in bipolar cells, evidenced by accumulation of DSCAM protein in the cell body. Abbreviations: Csen: calsenilin. Scale bar in H = 20 μm. Scale Bars in J-L = 50 μm. Scale bar in M = 20 μm. Insets in J-K = 25 μm box.

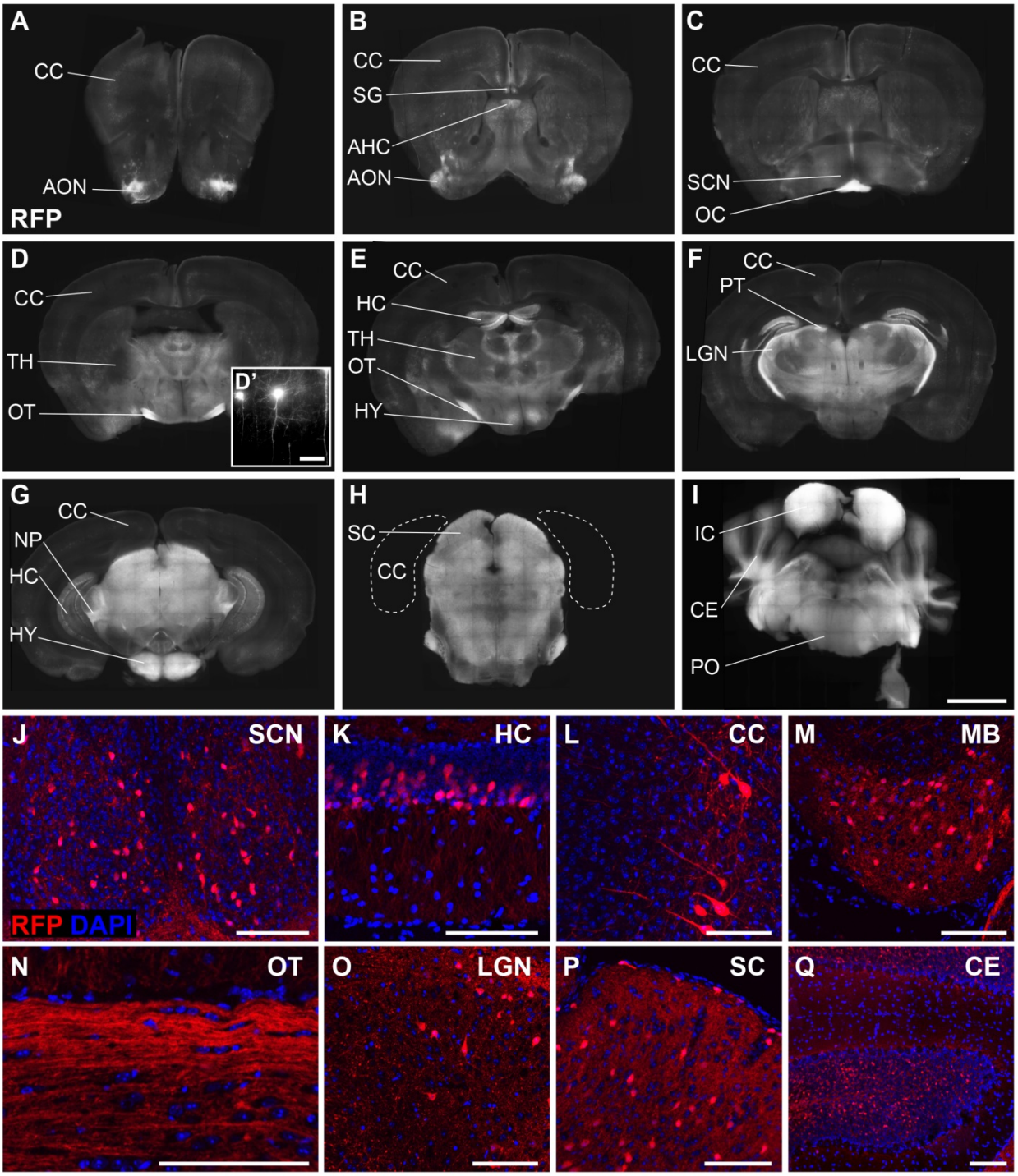

Figure 3.2. *Pou4f2*^{Cre} mediated recombination within the brain. Cre mediated recombination within the brain was assayed in vibratome and cryo-sections of *Pou4f2*$^{Cre/+}$ Ai9 mice. **A-I,** in vibratome sections, reporter activity was detected throughout many regions of

the brain. **D',** high magnification image showing pyramidal cells targeted by Cre. **J-Q,** in cryosections, reporter activity was found within retina ganglion cell axons projecting throughout the brain, but was also found within neural cell bodies and neurites within the brain, within many different regions. Abbreviations: AHC—Anterior Hippocampus, AON—Anterior Olfactory Nucleus, CC—Cerebral Cortex, CE—Cerebellum, HC—Hippocampus, HY—Hypothalamus, IC—Inferior Colliculus, LGN—Lateral Geniculate Nucleus, MB—Mammillary Body, NP—Nucleus Peduncularis, OC—Optic Chiasm, OT—Optic Tract, PO—Pons, PT—Pretectum, SC—Superior Colliculus, SCN— Suprachiasmatic Nucleus, SG—Supracallosal Gyrus, TH—Thalamus. Scale Bar in D' = 50 μm. Scale Bar in I = 2 mm. Scale Bars in J-Q = 100 μm.